General Changes

In addition to the changes made directly in response to the referees' comments, which are detailed separately, we have made several other changes to improve the clarity/completeness of the presentation, primarily in the figures (accompanied by minor modifications in the text). We describe below the changes made to the figures, and the motivation for them. None of these changes alters our conclusions in any way; we hope that they improve the clarity of the presentation.

Figure 1 (490 K Polar Processing Diagnostics)
We have removed the timeseries of V_{NAT}/V_{vort} (panel b in old figure) since the information provided in panel a (minimum temperatures) and Figure 3 lead to the same conclusions (this was suggested by referee #3). We have also simplified the sunlit vortex area panel (panel d in old figure; now panel c) by including the total vortex area only for 2015/16 (thin red line), and adding the daily climatological maxima of MERRA-2 vortex area (the topmost thin black line) to help make our point that the 2015/16 vortex was unusually large for most of the season.

Figure 3 (Winter Polar Processing Statistics)
We have removed the vertically summed number of days below PSC thresholds (panels b and d in old figure) since the information provided in those panels was mostly redundant with the combination of that given by the minimum temperatures shown in Figure 1a and the winter mean V_{PSC}/V_{vort}. We have also added error bars that represent the sensitivity of the winter mean volume diagnostics to the PSC thresholds used. The upper extent of the error bars represent winter mean V_{PSC}/V_{vort} calculated using temperature thresholds with $T < (T_{PSC} + 0.5\ K)$, whereas the lower extent of the error bars represent the same but for temperature thresholds with $T < (T_{PSC} - 0.5\ K)$.

Figures 9 - 11 (MLS and function M maps + M vs sPV scatterplots)
We have done our best to increase the visibility of the continent outlines and latitude/longitude divisions on all the maps. To aid this on the function M maps, we changed the vortex edge PV contours on these maps to cyan (so as not to interfere with the gray continent outlines and white latitude/longitude sectors). We also change the PV contours overlaid on the function M maps (third row in each figure). In the old versions of the figures, we used contours from the 12UT MERRA-2 PV fields, which were slightly misaligned with the function M maps that use data from trajectories initialized at 00UT. As a result, we now show 00UT PV contours on the function M maps.

Figure 14 (Multi-vortex time series)

We have changed the colors to improve clarity, and to be consistent with the color changes to Figures 12 and 13 described in our responses to the reviewers. Now, the black, blue, and green lines correspond to the correct vortex regions in Figures 12 - 13, and the transients are properly labeled at both 490 and 550 K (before, the short-lived blue vortex at 550 K in late March was erroneously labeled “third”). The bulk quantity has also been changed from gray to orange to prevent confusion with the gray envelopes used for the black (parent) vortex.

We also changed the names of the vortices to use a consistent terminology throughout. We refer to the small offspring regions as offspring-p (green) for “persistent offspring” or offspring-s (blue) for “short-lived offspring”. Offspring that persisted for less than about a day are referred to as “transient”. The Figure 14 legend has been changed to reflect this.

Finally, the vortex-edge averaged windspeed panels (second row) now use quantities that are derived from an improved edge-following algorithm in CAVE-ART, which gives us a more accurate estimate of the average windspeeds and their variability around the edge (we have thus now included standard deviation envelopes on these lines). The differences between the old version and the new version are minor, and none of our conclusions or statements are affected by the change.

Supplementary Animation 1 (CAVE-ART Identification of Vortices)
We have increased the number of days that the animation covers to include all of 1 Feb through 30 Apr. We also changed the PV colormap and map projection (now orthographic) to better contrast regions with high and low PV. Furthermore, the vortex edge contours are now plotted using the CAVE-ART masks to omit the small high PV regions that exceed our sPV edge thresholds.

Equivalent ellipses are now colored to be consistent with Figures 12 - 14 in the main paper. Finally, we inverted the colors of the background and text so that the background is black and the text is white (to be more viewer friendly).

Interactive comment on "The major stratospheric final warming in 2016: Dispersal of vortex air and termination of Arctic chemical ozone loss" by Gloria L. Manney and Zachary D. Lawrence

A. Dörnbrack (Referee)

This paper is a well-written, comprehensive study of the fate of the northern hemispheric polar vortex in spring 2016. The paper is well-structured into an Introduction, a Data and Method section, overviews the 2015/2016 polar vortex evolution in Section 3, and, finally, focusses on the early vortex breakup in March 2016 and the subsequent mixing of vortex air with mid-latitude air. Section 5 summarizes and concludes the paper with clear statements and with a friendly wink and hint to follow the NH vortex evolutions in the future with care. I'm sure, the authors will do so as they possess the suitable diagnostic tools to analyze global satellite and meteorological data in an efficient way.

The Arctic winter 2015/16 was extraordinarily cold and the vortex-wide temperatures felt as low that the conditions in January resembled those of the Antarctic in terms of chemical composition and PSC appearances. Besides the fascinating subject of the recent winter, it is the clarity in structure and writing which make the paper a joy to read.

The Introduction sets the scene by stating "that SSWs affect Arctic lower stratospheric chemical ozone loss in ways much more complex than a simple association of low (high) temperatures with more (less) ozone loss". So it is consequent to read the motivation as: "Thus, understanding the complex relationships between SSW dynamics, stratospheric vortex evolution, and chemical composition and processing, is critical to diagnosing and predicting ozone loss and recovery in the Arctic and its climate consequences." After a short historical view, the authors come back to the topic by discussing the interannual variability of NH winters (minor/major SSWs and dates of final warmings) in close relation to the chemical ozone loss. Some of the main results are already anticipated in the fourth paragraph: (1) "the 2015/16 Arctic winter was the coldest on record (since at least 1979)"; by the way, Matthias et al. (The extraordinarily strong and cold polar vortex in the early northern winter 2015/16, GRL, under review) showed that it is was indeed the coldest in the recent 68 years. (2) a major final warming "beginning in early March 2016 resulted in the breakup of and dispersal of chemically processed air from the vortex, which halted chemical loss much earlier than in 2011".

Section 2 reviews the data sources and the methods. It is impressive to see that the

latest versions of MERRA-2 and MLS data are used. The diagnostic quantities and tools are presented systematically. Even newer developments which are in the pro-cess of publishing are explained in a comprehensive way. The authors apply a broad spectrum of well-established and newly developed diagnostics to quantify the spatio-temporal variation of the various trace gases and dynamical quantities specifying the mixing in the surf zone of the polar vortex.

The Overview of the 2015/16 vortex evolution and composition focusses on thermal and chemical aspects. For a reader not so familiar with all the peculiarities of the previous winters less direct comparison would be advantageous. Maybe, sentences like (around line 320) "Ozone continued to decrease in the vortex at a rate slightly faster than that in 2011 until the beginning of March 2016. If uninterrupted, ozone values would have been expected to drop lower than those in 2011 by mid-March." could be slightly reformulated to give for example explicit values of rates. But this, for sure, is only a matter of taste. At the end, main results for the winter 2015/16 (in relation to previous ones) are presented and key words are: "leading to unanticipated extremes in Arctic polar processing, the 2015/16 winter stands out as yet another unexpected extreme in variability of the Arctic winter stratosphere." , "The period of over a month, from late December through early February, with temperatures below the ice PSC threshold was unprecedented in the Arctic", "much greater degree of dehydration", and "extreme denitrification", "extensive early winter chlorine activation", and "chemical ozone loss began early". And finally, we read: "Thus, the critical factor resulting in less ozone loss than in 2011 was the much earlier increase in temperatures and vortex breakup in 2016."

The Section 4 about the 2015/16 major final warming and the resulting vortex breakup and mixing exemplifies the trace gas evolution and the strength of the transport barrier, and the mixing especially in the surf zone by refined analyses at different isentropic surfaces representing the conditions in the middle and lower stratosphere. I'm not the expert to evaluate the details of the applied diagnostics but the text reads logical and the conclusions are based on well-funded results from the respective simulations. Altogether, the paper can be published in the present form!

Initial Reply, Posted 7 Sep 2016

We thank Dr. Andreas Dörnbrack for his very positive review, and are glad that he enjoyed reading the paper -- we certainly enjoyed writing it, and are pleased to hear from someone who

appears to share our fascination with the unpredictable wide range of variations in Arctic stratospheric meteorology.

With regard to Section 3, the overview of the 2015/2016 vortex evolution and composition, we do appreciate that this material could be a little hard to follow for the reader who is not already familiar with the conditions and amounts of ozone loss in other recent winters. When we revise the paper, we will work on being more explicit about the conditions and ozone loss amounts / timing in the previous winters that are highlighted, so it is easier for the reader to follow the comparisons.

Added author comment, 26 Oct 2016:

In addressing the other referees' comments, we have made several clarifications to Section 3, primarily to note more explicitly the connections between the meteorological diagnostics shown in Figures 1 and 3 and the trace gas evolution shown in Figure 2, and to make the motivation of the comparisons with the previous winters clearer. We believe this last point will help to address the slight confusion Dr. Dörnbrack indicated in the comparisons with other winters.

Interactive comment on "The major stratospheric final warming in 2016: Dispersal of vortex air and termination of Arctic chemical ozone loss" by Gloria L. Manney and Zachary D. Lawrence

Anonymous Referee #3

Received and published: 9 September 2016

This paper is certainly comprehensive, appropriate for ACP and most probably, correct. It was, however, also difficult to read and review. It comes across, at least to this reviewer, as a so-called "core dump" of information. As a consequence, I readily admit that this review is probably incomplete and that I probably missed pieces of information that to the authors, at least, they would deem critical. My comments are therefore (with one exception) more editorial than scientific.

We thank the referee for their valuable comments regarding our manuscript. As we describe below and in our responses to the other reviewers, we have made numerous modifications that we hope clarify our paper and elucidate how the information we have included is focused on a comprehensive analysis of the major final warming in 2016.

General 1. One general science question that I think could use a greater exposition is the question of the MFW. The authors imply that this hybrid event in 2016 is unusual. Some context as to its occurrence frequency would be helpful. Is this the first to occur in the AURA record?

This event was not the first in the Aura record; the 2004/2005 Arctic winter was similar in that its unusually cold conditions were cut short by an early final warming around 10-12 March 2005. However, 2015/2016 was much colder, and the potential for polar processing more severe. In addition, final warming events as early as these are uncommon. According to the table provided in Hu et al., 2014, only 13 winters between 1958 and 2012 had early final warmings before 1 April, of which only 5 occurred before March 15. We have included additional text in our conclusions section that discusses these points, including differences and similarities in the 2005 and 2016 events.

2. As far as presentation, Section 3 is a case in point as exemplifying my concerns. Figures 1-3 are introduced in rather random order, with lots of information, which, while not technically wrong, may well be irrelevant. The authors present a whole bunch of figures (14 panels in all for Figures 1-3) and then jump back and forth in a scatter shot discussion. This is very taxing to read. The first three paragraphs do not even discuss the 2015-16 season, but rather present a literature review of 3 three previous winters.

Line 27 on page 7 is a good example. The statement is simple- temperatures in a particular year (a year which was not the subject of the present paper) were cold enough to activate chlorine for a prolonged period of time. So why do we need to refer to four separate figure panels (Figure 1a and b Figure 2d and e?) to make this simple point (which again is irrelevant to the subject of this paper that is nominally about 2016)? In fact, I don't understand why Figure 2 is referred to here. Is it because ClO was going up? That is not explained.

We have made several revisions to section 3, including adding text to clarify that we are discussing Figures 1 and 2 together so that we can draw the direct connection between the meteorological diagnostics and the implications of their evolution for changes in the trace gases (e.g., minimum temperatures are directly related to the evolution of HNO3 and H2O via PSC formation and denitrification/dehydration; these are in turn linked to chlorine activation and deactivation; sunlight exposure shown in Figure 1 is directly linked to elevated ClO and ozone loss shown in Figure 2; etc). By discussing these figures in a unified way, we elucidate the dependences of the composition on the meteorological conditions. We have also simplified Figure 1 by removing the V_{NAT}/V_{Vort} panel, which the referee points out below provided little additional information, and reducing the number of lines on the sunlit vortex area panel (now Figure 1c).

3. Adding up all the panels in 15 figures, the paper contains 128 separate graphs. I confess that I found it difficult to subject each and every one to the scrutiny they probably deserve; I do nonetheless strongly suspect that they are not all necessary. As an example, I did examine one specific panel- that of Figure 1b. All references to Figure 1b occur with a simultaneous reference to Figure 1a. I therefore conclude that Figure 1b can't be necessary since it never is referred to independently of Figure 1a. So it should be deleted. Especially since they never describe it (what is V_nat/V_vort?-they briefly mention it on page 9, but not in the context of Figure 1).

We have reduced figures and figure panels where possible, including removing the panel in Figure 1 that the reviewer mentioned as a candidate for deletion. In addition, we have removed two panels of Figure 3, all of Figure 12 (four panels), and four panels in each of Figures 13 and 14 (now Figures 12 and 13). We do stress, however, that one of the main points of our paper is that there is good agreement between the dynamics (represented by diagnostics derived from MERRA-2) and chemistry/transport as seen by measurements from MLS, which all paint a consistent picture of what happened throughout the 2015/16 Arctic winter season, and in order to make this point, we need to show these fields and their evolution. Every figure panel that is included in the paper is used to support some point; a majority of them are referred to not only when initially

discussed, but also referred back to to support points made about or show consistency with succeeding figures.

4. I also think Figure 3 is unnecessary. Not that it's technically incorrect, but it adds no new information that is not conveyed in Figures 1 and 2. Indeed, their concluding sentence on lines 19-20 of page 9 can easily be gleamed from Figures 1-2.

As per our reduction of figure panels mentioned above, we have removed the panels showing the vertically summed number of days below the PSC thresholds. We now only show the winter mean V_{NAT}/V_{Vort} and V_{ice}/V_{Vort}. Although there is some overlap with the information conveyed in Figures 1 and 2, Figure 3 is still necessary to show that the winter mean polar processing and ozone loss potential in 2015/16 was unusually large, comparable to that in 2011; this point cannot be seen by looking at Figure 1 alone.

Minor

1. Figures 5-14 (with the exception of Figure 8) are essentially 3 sets of three figures for 850, 490, and 550 potential temperature surfaces. It would be introductory few sentences at the beginning of Section 4 explaining why they chose these three levels. Even if it was empirically determined that they were good representative levels, they should at least say that. As it reads, it just says (for example) Figures 5-7 without telling the reader where you are going with this. You have to read almost 2 pages of the draft before you find out that these 3 figures are for three separate altitudes.

At the end of section 3, we have a transition paragraph that points out the three levels we are going to focus on in section 4 and their significance. In addition, we have added text at the beginning of section 4 noting that parallel figures are going to be shown at three levels to contrast/compare their behavior.

2. Figure 6 vs Figure 7. If I understand correctly, the text on page 11 suggests (line 25, compared with line 7) that one difference is that N2O and O3 do not show mixing out of the vortex at 550K but they do at 490 K. Looking at Figures 6c and 7c, I see no difference. Am I supposed to?

We apologize for a lack of clarity in these statements. The main point in the paragraph on 550K was the consistency of persistent strong trace gas gradients along the vortex edge with the stronger persistent transport barrier seen in PV gradients and K_{eff} at this level. This does indeed imply less mixing out of the vortex at 550K than at 490K. We have revised the text to clarify both points.

3. Figure 1c: what is Max PVG? Those three letters do not appear anywhere else in the text or figure captions.

We apologize for this oversight; max PVG stands for “maximum PV gradients.” We have changed the text in the Figure 1 caption to read: “maximum gradients of scaled potential vorticity as a function of EqL (Max PVG) ...” to make this clear.

4. Figure 15: What do the colors mean? There is a label that says “first”, “second” etc, but doesn’t explain what those terms mean other than “bulk”. Are they related to the colors of various fragments in Figure 14. If so, it should say so.

We have clarified our references to the colors and the regions in the text. Rather than referring to the offspring regions as first, second, etc, we now refer to them as “parent”, “offspring-p”, and “offspring-s” to describe the amount of time these regions existed (the “p” and “s” in offspring-p and offspring-s stand for “persistent” and “short-lived”, respectively). Vortices that persisted for about a day or less are labeled “transient”. We have also added text to the Figure 14 caption to explain these names/references, and they are explained in the text where they are first introduced (in conjunction with Figures 10 and 11).

5. Abstract: Line 20. Where do they show chlorine in the offspring vortices? Figure 15 does not show chlorine. There are cryptic references to chlorine activation and deactivation scattered throughout the text, but I could not find where it pointed to a figure saying “this shows the deactivation of chlorine etc. etc.”

We note explicitly in the text related to Figure 14 regarding shorter lived species that the average values of ClO, HCl, and HNO3 are very similar across the parent and offspring vortices, and hence showing the evolution in individual vortices (as in Figure 14) would only add panels without adding information. We have added text explicitly noting that how ClO evolves in each vortex can be deduced from Figure 2e. Also, the time evolution of ClO is shown clearly in Figures 4e and 6e.

Interactive comment on "The major stratospheric final warming in 2016: Dispersal of vortex air and termination of Arctic chemical ozone loss" by Gloria L. Manney and Zachary D. Lawrence

R. Thiéblemont (Referee)
remi.thieblemont@latmos.ipsl.fr
Received and published: 19 September 2016

This paper provides a thorough description of the evolution of the 2015/2016 Northern Hemisphere stratospheric winter until the breakup of the polar vortex and the dispersal of its fragments. This winter was unique: while it initially presented the characteristics for an unprecedented ozone loss (i.e. prolonged temperatures below ice polar stratospheric cloud thresholds), an anomalous early and strong major final warming interrupted the ozone depletion process. Dynamical and chemical processes are characterized using Microwave Limb Sounder satellite trace gas measurements, and advanced mixing and polar vortex diagnostics derived from meteorological reanalysis. This case study of the winter 2015/2016, and its comparison with the series of singular recent winters, very well illustrates the complexity of the dynamical and chemical interactions that drive Arctic ozone depletion. In my opinion, this paper is important as it further contributes to showing that each Arctic winter season is unique and that substantial research efforts are needed to better understand their extreme variability and the consequences of this variability (e.g. on ozone depletion, stratosphere/troposphere couplings). The methods and diagnostics used in this study are scientifically sound and relevant. The analysis is very carefully conducted. My main criticism rather concerns the form: the main text and its figures are extremely dense and contains a lot (too much?) of information so that it is sometime hard to differentiate what is important from what is more anecdotal. While in some places the degree of detail seems to me exaggerated (e.g. p10l32-p11l10 where tracer extrusions are discussed while not really obvious), in other places, including further details may help to make the paper easier to follow (see comments below).

Motivated both by this comment, and those of Referee #3, we have gone through the paper with a focus on assessing the clarity and necessity of the text and each figure/figure panel. As a result, we have eliminated several figure panels that were not as critical to our message, and clarified the text to indicate the motivation for showing the information that is included.

Regarding the particular example given above of the discussion of filamentation in relation to Figure 6, we have revised and reduced this discussion to eliminate details that are less critical to the paper.

Hence in my opinion, this paper is suitable for publication in Atmospheric Chemistry and Physics after consideration of the specific (minor) comments and suggestions provided below.

We thank Dr. Thiéblemont for his careful and thorough review, and very helpful comments on our paper.

Specific comments:
1) p3l32: Typo change "MERRRA" to "MERRA"

Done.

2) p4l20: Please provide further detail on the way the potential vorticity is scaled. The sPV is widely used throughout the paper so few precisions about it may be useful for the readers.

Changed to "... (sPV, scaled to have a similar range of values throughout the stratosphere using a standard atmosphere value of static stability, as in Dunkerton and Delisi, 1986; Manney, et al, 1994) ..."

3) Diagnostics (i.e. sections 2.3 & 2.4): This paper makes use of a very high number of diagnostics to describe mixing processes, transport, vortex size and so on. Although the different diagnostics are very well explained in the main text, non-expert reader may quickly be lost once the description of the (dense) analysis begins. The authors may consider adding a table which gives a summary describing (briefly) the different diagnostics and their usefulness.

We have added a list that summarizes the transport and mixing diagnostics we use at the end of section 2.4. While we did not do the same for the polar processing diagnostics in section 2.3, we did remove some of the diagnostics previously shown in Figures 1 and 3, and added more explicit text clarifying how each diagnostic is related to the evolution of trace gases in the polar vortex. We hope this helps reduce the complexity, and makes the motivation for including each diagnostic clear.

4) p7l25: "The 2010/2011 winter". Please mention the associated color line in bracket to help the reader.

A note with the line colors has been added the first time each year is mentioned.

5) p8l1: "In early January 2013". Same here, please mention the associated color.

A note with the line colors has been added the first time each year is mentioned.

6) p8l2: "strongest "vortex-split" SSWs on record" What does strong mean here? What defines the strength of a SSW (persistence, temperature, vertical extension?)? Please clarify.

We have revised the text to indicate that we mean among the largest abrupt temperature increases, deepest range of wind reversals, and most prolonged periods of easterlies.

7) p8l6: "2014/2015". Please mention the associated color.

A note with the line colors has been added the first time each year is mentioned.

8) p8l6: "brief minor SSW". Please give the date. (I guess early January)

The date has been added: "...very brief minor SSW (with a brief vortex split on 5~January~2015)..."

9) p8l13: Typo change "though" to "through"

Done.

10) p8l14: "unprecedented". On MERRA record? Please clarify.

We now specify that it is in the MERRA-2 record: "...unprecedented in the Arctic, where the MERRA-2 record rarely shows more…"

11) p8l31: "in 2015/1016, 2012/2013, and 2010/2011". Why not 2014/2015?
The green curve looks similar in early winter on Figure 2a.

This is indeed true if the period is limited to early winter, and we now simply state that it was similar in all the years highlighted.

12) p11l1-2: "This is consistent [...] anticyclone during this period". Does anticyclone

refer to the Aleutian High here? Please clarify.

We have modified this to note that we do, indeed, mean the Aleutian anticyclone.

13) Figure 8: Please replace y-axis "Effective diffusivity" by "Keff" to be consistent with the main text (p11l30).

We have labeled the y-axis in Figure 8b, as well as the color bars in Figures 5--7b, "Effective Diffusivity (K_{eff})".

14) p11l33: "Keff and M minima" Is it not rather M maximum? M maximum -> vortex edge -> transport barrier.

Thanks for catching this error. We have revised it to say "...sPV gradient and *M* maxima, K_{eff} minima, and strongest trace gas gradients…"

15) Figure 9-14: Please make the continents more visible on maps and provide at least on longitude coordinate. Otherwise it is quite hard to follow Figures together with the main text and the geographical location that are refereed (e.g. Alaska p13l7 but also at other places).

We have done our best to make the continents and latitude/longitude lines more visible in all cases. In addition, we have provided an orientation reference in the first figure caption for each type of map, noting that 0 degrees longitude is at the bottom of the maps and 90 degrees E to the right.

16) P13l12: "in the anticyclone.". Is it not "in the edge of the anticyclone" that the M values are the strongest?

It is both along the edge and along the persistent filaments that spiral into its interior; the text has been modified to reflect this.

17) At 550 K, a doubled vortex edge appears in the main vortex fragment (see Fig 11, 14) from beginning of April. Is this an artifact or a real structure? Please comment on this.

It is difficult to say whether the doubled-edge structure is real or an artifact since it represents the sPV dropping slightly below our vortex-edge threshold in the core of the fragment. However, we do not think it has any particular significance in relation to

transport/mixing in this case, since the M maps show that the highest M values are around the outer edge. We have added additional text stating this.

18) Figure 13-15 (and associated text). The green and blue offsprings seem actually switched between the 490 and 550 K levels. If indeed this is the case, it may be confusing. Therefore, it may be more relevant to keep the same color for the upward extension of the same offspring.

We have switched the colors of the vortices so those of the smaller offspring that persist longest (and are the extension of the same vortex in the vertical) are the same color. We now label the vortices as "parent," and "offspring-p" and "offspring-s" for the "persistent" and "short-lived" small vortex regions, respectively. (Offspring vortices that persisted about a day or less are labeled and described as "transient".)

19) p15l17-19: May this vortices coherence dependence with height be partly related to differences in diabatic processes with height?

We do believe this to be the case. There is a large body of literature showing that most final warmings proceed from the top down, and this is largely related to shorter radiative timescales in the middle to upper stratosphere. However, in removing material that, though interesting, seemed peripheral to our primary focus, we have deleted the statement that raised this question; therefore we have not modified the text in this regard.

20) p16l7: "begins dropping earlier,": earlier than when? Please clarify.

We meant "begins dropping earlier than the vortex area…" and have added this to the text.

21) p16l7: "period between the beginning of the MFW and the split": is it the period between the two dashed lines? Please clarify.

Yes, we have added a note saying this in the text: "...period between the MFW and the split (between the two vertical dashed lines in Figure 14)..."

22) p16l19-21: "In fact, as seen in Figure 13, a coherent mass of air from the blue vortex persisted into April – represented in Figure 15 by the individual purple points labeled "transient". I guess these transient vortices are those seen in the supplementary animation and labelled 4, 5, 6, 7 and 8 at the 490 K. If yes, please mention it.

You are correct, and we have added text pointing this out and referring to the animation in the discussion of Figure 14 (was Figure 15).

23) p18l8: "one previous winter.". Please recall which winter it is.

We have added this information: "...one previous winter (2012/2013, Figure 2d--f)..."

24) P20l1-2: "This is particularly interesting given reported differences between years with early and late Arctic final warmings, which have not, in general, accounted for the suddenness of those final warmings (e.g. Waugh and Rong, 2002; Akiyoshi and Zhou, 2007);". In recent studies on Frozen-In Anticyclones (FrIACs), tracer transport was linked to the suddenness/abruptness of final warmings (see e.g. Allen et al. (2012), Thiéblemont et al. (2013) or Thiéblemont et al. (2016)).

This is a very good suggestion; indeed we were remiss in not mentioning these studies. We have added a brief discussion of FrIACs following sudden/abrupt final warmings in this paragraph.

We would like to thank Drs. A. Ruiz-Herrera and A. M. Mancho for their comments regarding Lagrangian descriptors and the Function M (hereinafter referred to as M). Clearly there is an ongoing discussion about cases for which Lagrangian descriptors (including M) are applicable diagnostics for elucidating flow characteristics. Although neither Dr. Ruiz-Herrera nor Dr. Mancho have suggested changes to our manuscript, we would like to expound upon our use of M, and specifically why we think it provides useful information beyond that given by the other transport barrier/mixing diagnostics used in our analysis of the 2015/2016 Arctic winter.

We have applied M to the stratospheric polar vortex, which is a well-understood system in the atmospheric sciences. There is a large body of literature that has established that the polar vortex edge, or polar night jet, acts as a significant transport barrier that dynamically and chemically separates intra-vortex air from extra-vortex air (e.g., Schoeberl et al., 1992). Maps of M in the polar winter stratosphere highlight this dynamical separation. Because high/low values of M represent the “long/short” distances traveled by parcels advected by the flow, we know that the band of high M values in the vortex edge region represents the position, strength, and approximate width of the polar night jet (see, e.g., Fig 9 in our paper). This band separates two regions with low M values -- the intra- and extra-vortex air. As the polar vortex weakens and shrinks, M values in this band are reduced to the point where there is no qualitative separation that significantly distinguishes intra- and extra-vortex air (e.g., in Fig 9, 4th column, 3rd row).

Furthermore, when binned as a function of potential vorticity (PV)-based equivalent latitude (EqL), M agrees well with other instantaneous transport barrier/mixing diagnostics. Maxima in M as a function of EqL correspond well with maxima/minima features in PV gradients, trace gas gradients, and effective diffusivity (see Fig 8 in our paper). This is no surprise since, as explained above, the largest M values occur in the vortex edge region where PV gradients are largest. Hence, M is at least as useful as these other instantaneous diagnostics, even though it incorporates 30 days’ worth of flow information (when using tau = 15 days).

Having established this agreement, M in addition allows us to examine local changes in transport and mixing that the other diagnostics, which are inherently calculated as averages around EqL contours, do not. And this in particular is what we find to be most useful about M in our context; it incorporates a history of the underlying dynamics. Investigation of instantaneous wind fields alone, for example, results in qualitatively similar maps to those of M, but M highlights the dynamical significance of short and long-lived features such as the vortex edge and vortex filaments. For example, parcels initialized within the vortex edge region obtain large values of M because, in the reverse trajectories, they very likely *originated in* the vortex edge, and in the forward trajectories, very likely *stay in* the vortex edge. Similarly, parcels initialized or drawn into a vortex filament obtain relatively large values of M because, in the reverse trajectories, they also very likely originated in the vortex edge -- but they don’t reach vortex-edge levels of M because at some point they are drawn off and stirred out in the surf zone.

Our simple/visual “distance travelled” interpretation is largely qualitative, but we think it is intuitive and helps prove our point that the 2015/2016 Arctic polar vortex decay was unusually intense and rapid, especially in light of the unusual strength and size of the vortex before the major final warming. As Dr. Mancho pointed out, we are using M in a different manner, in a way that we think does not depend on the mathematical rigour necessary for discussing flow manifolds, hyperbolic trajectories, etc.

We have included in our manuscript additional references to the literature highlighting the use and criticisms of Lagrangian descriptors pointed out by Drs. Mancho and Ruiz-Herrera. Furthermore, we have added text to our manuscript to clarify our use of M and why the ongoing discussion surrounding Lagrangian descriptors does not affect our simple use of M.

References

Schoeberl, M. R., L. R. Lait, P. A. Newman, and J. E. Rosenfield (1992), The structure of the polar vortex, J. Geophys. Res., 97(D8), 7859–7882, doi:10.1029/91JD02168.

The major stratospheric final warming in 2016: Dispersal of vortex air and termination of Arctic chemical ozone loss

Gloria L. Manney[1,2] and Zachary D. Lawrence[2]

[1]NorthWest Research Associates, Socorro, New Mexico, USA.
[2]Department of Physics, New Mexico Institute of Mining and Technology, Socorro, New Mexico, USA.

Correspondence to: Gloria L Manney (manney@nwra.com)

Abstract. The 2015/16 Northern Hemisphere winter stratosphere appeared to have the greatest potential yet seen for record Arctic ozone loss. Temperatures in the Arctic lower stratosphere were at record lows from December 2015 through early February 2016, with an unprecedented period of temperatures below ice polar stratospheric cloud thresholds. Trace gas measurements from the Aura Microwave Limb Sounder (MLS) show that exceptional denitrification and dehydration, as well as extensive chlorine activation, occurred throughout the polar vortex. Ozone decreases in 2015/16 began earlier and proceeded more rapidly than those in 2010/11, a winter that saw unprecedented Arctic ozone loss. However, on 5–6 March 2016 a major final sudden stratospheric warming ("major final warming", MFW) began. By mid-March, the mid-stratospheric vortex split after being displaced far off the pole. The resulting offspring vortices decayed rapidly preceding the full breakdown of the vortex by early April. In the lower stratosphere, the period of temperatures low enough for chlorine activation ended nearly a month earlier than that in 2011 because of the MFW. Ozone loss rates were thus kept in check because there was less sunlight during the cold period. ~~And although~~ Although the winter mean volume of air in which chemical ozone loss could occur was as large as that in 2010/11, ~~net chemical ozone loss was considerably less.~~ observed ozone values did not drop to the persistently low values reached in 2011.

We use MLS trace gas measurements, as well as mixing and polar vortex diagnostics based on meteorological fields, to show how the timing and intensity of the MFW and its impact on transport and mixing halted chemical ozone loss. Our detailed characterization of the polar vortex breakdown includes investigations of individual offspring vortices and the origins and fate of air within them. Comparisons of mixing diagnostics with lower stratospheric N_2O and middle stratospheric CO from MLS (long-lived tracers) show rapid vortex erosion and extensive mixing during and immediately after the split in mid-March; however, air in the resulting offspring vortices remained isolated until they disappeared. Although the offspring vortices in the lower stratosphere survived longer than those in the middle stratosphere, the rapid temperature increase and dispersal of chemically-processed air caused active chlorine to quickly disappear. Furthermore, ozone-depleted air from the lower stratospheric vortex core was rapidly mixed with ozone rich air from the vortex edge and midlatitudes during the split. The impact of the 2016 MFW on polar processing was the latest in a series of unexpected events that highlight the diversity of potential consequences of sudden warming events for Arctic ozone loss.

1 Introduction

Sudden stratospheric warmings (SSWs), which are characterized by abrupt warming and weakening or reversal of the polar wintertime westerly circulation (e.g., Andrews et al., 1987, and references therein), lead to extreme variability in Northern Hemisphere (NH) polar temperatures, as well as in the structure, evolution, and intensity of the Arctic stratospheric polar vortex. SSWs are in part responsible for the smaller potential for ozone loss in NH than in Southern Hemisphere (SH) spring (e.g., Andrews, 1989; WMO, 2014). SSWs are relatively common in the NH, occurring at a rate of ∼0.6 events per year by many common definitions (see, e.g., Butler et al., 2015, and references therein). However, recent studies have shown that SSWs affect Arctic lower stratospheric chemical ozone loss in ways much more complex than a simple association of low (high) temperatures with more (less) ozone loss (Manney et al., 2015a, b, and references therein). Thus, understanding the complex relationships between SSW dynamics, stratospheric vortex evolution, and chemical composition and processing, is critical to diagnosing and predicting ozone loss and recovery in the Arctic and its climate consequences.

Recent Arctic winters with SSWs have led to different extremes in polar processing and ozone loss: The 2012/13 NH winter was exceptionally cold in December, but a major vortex-split SSW in January gave rise to two unusually strong offspring vortices that moved far into sunlight (Manney et al., 2015a). The combination of extensive polar processing activity prior to the SSW and ample sunlight exposure following the SSW led to the earliest onset of rapid Arctic ozone loss in the 12-year record from the Aura Microwave Limb Sounder (MLS); that loss continued through the end of January (when the polar vortex dissipated completely). In contrast, polar processing was effectively halted in the NH winter of 2014/15 by a brief minor SSW in early January (Manney et al., 2015b). Although the minor SSW had similar signatures to a major SSW in the middle and upper stratosphere, it left the lower stratospheric vortex virtually unscathed except for causing temperatures to rise above chlorine activation thresholds for a couple of weeks. This resulted in anomalously little chlorine activation, and the highest wintertime ozone seen in the twelve-year MLS record.

Interannual variability in NH winters is also reflected in the timing of the springtime stratospheric final warming. These events mark the transition of the stratospheric winter circulation from westerly to easterly, where it remains until the following autumn. Numerous studies suggest that the timing of final warmings is related to SSWs earlier in winter: Labitzke (1982) showed that final warmings following major SSWs in January or February in the 1950s through 1970s were usually delayed due to late winter cooling after the SSW; recently, Hu et al. (2014) showed a statistically significant relationship between midwinter (December through March) major SSWs and late (∼April and May) final warmings. The converse is also true in that many early final warmings tend to occur in winters without a prior strong SSW (Labitzke, 1982; Hu et al., 2014, and references therein). The end of any potential for polar processing and chemical ozone loss typically closely follows the final warming, as temperatures rise above activation thresholds and the breakdown of the polar vortex rapidly disperses chemically processed air, both of which hasten chlorine deactivation (e.g., Prather and Jaffe, 1990; Tan et al., 1998; Santee et al., 2008, and references therein). Because of this interplay of chemical/microphysical and dynamical processes, the abruptness and timing of the final warming plays a substantial role in polar processing, and there is large interannual variability in the evolution of final warmings (e.g., Black and McDaniel, 2007). Labitzke (1982) first noted that SSWs in late February or March often turn

directly into final warmings. Such an early and abrupt final warming, initiated by a major SSW early enough in the season that recovery is possible, but after which recovery does not occur, is referred to as a major final warming (MFW) (see, e.g. Hoffmann et al., 2002; Labitzke, 2002; Naujokat et al., 2002; Manney et al., 2006a, b; Blume et al., 2012). MFWs can result in more rapid mixing of air from the polar vortex than later, more gradual final warmings (e.g., Waugh and Rong, 2002; Akiyoshi and Zhou, 2007), and rapid cessation of ozone loss (e.g., Konopka et al., 2003; Marchand et al., 2004; Manney et al., 2006b).

As we will show below, the 2015/16 Arctic winter was the coldest on record (since at least 1979) in the lower stratosphere through January. Minimum temperatures in the lower stratosphere were far below those in the 2010/11 winter/spring when extensive chemical loss led to record low values of Arctic ozone in April 2011 (Manney et al., 2011; WMO, 2014, and references therein). There was thus the potential for extreme chemical ozone loss that might have exceeded that in 2011. However, an MFW beginning in early March 2016 resulted in the breakup of and dispersal of chemically processed air from the vortex, which halted chemical loss much earlier than in 2011. We show that the critical factor resulting in less ozone loss than in 2011 was the early final warming in 2016, presenting another instance when the occurrence of a major SSW (in this case an MFW) played a key role in determining the amount of ozone loss in an Arctic winter, in a way differing from the diverse scenarios we have already observed in recent years.

In this paper, we analyze meteorological data from the MERRA-2 (Modern Era Retrospective-analysis for Research and Applications) reanalysis and trace gas data from the Aura MLS instrument to give an overview of dynamical conditions and chemical composition in the polar vortex during the 2015/16 winter, and detail the effects of the MFW that shattered the vortex in early March 2016, which curtailed polar processing and limited chemical ozone loss. We focus on transport and mixing during the vortex breakup and its effects on the composition of air that was dispersed from the vortex. A comprehensive picture of the vortex evolution and breakup is obtained using a newly developed package for characterizing multiple vortices. We describe the evolution of the vortex and trace gases through the MFW and associated vortex splitting, focusing on mixing and dispersal of chemically processed air from the vortex.

After describing the datasets and methods used (Section 2), Section 3 provides an overview of the dynamical conditions and chemical composition of the vortex throughout the 2015/16 winter. Section 4.1 then provides an overview of the evolution of trace gases and relationships to bulk diagnostics of mixing and transport barriers. In Section 4.2, the synoptic/regional processes leading to these relationships are diagnosed. Section 5 gives a summary and conclusions.

2 Data and Methods

2.1 MERRA-2 Reanalysis

The National Aeronautics and Space Administration's (NASA) Global Modeling and Assimilation Office (GMAO) MERRA-2 dataset (Bosilovich et al., 2015) is a global reanalysis that covers the satellite era from 1980 to the present. It uses the Goddard Earth Observing System version 5.12.4 assimilation system with a cubed-sphere model to perform its analyses. As in its predecessor, ~~MERRRA~~MERRA, an incremental analysis update (IAU) (Bloom et al., 1996) applies the analysis tendency gradually over the 6-hour analysis window. MERRA-2 contains substantial upgrades over MERRA, including new input data,

model constraints, and parameterizations (Molod et al., 2015; Takacs et al., 2016). Assimilated fields are provided on a 0.625° × 0.5° longitude/latitude grid with 72 hybrid σ-pressure levels. Here we primarily use the wind, temperature, and potential vorticity fields provided in the "M2I3NVASM" file collection (Global Modeling and Assimilation Office (GMAO), 2015), the set of dynamically consistent fields obtained after the IAU step; these fields are provided at the full model resolution at 3-hour intervals (8 times per day).

2.2 MLS Data

The Earth Observing System (EOS) Aura satellite was launched in July 2004, in a 98° inclination orbit that provide data coverage from 82° S to 82° N latitude on every orbit. Aura MLS measures millimeter- and submillimeter-wavelength thermal emission from the limb of Earth's atmosphere. Detailed information on the measurement technique and the Aura MLS instrument is given by Waters et al. (2006). Vertical profiles are measured every 165 km along the suborbital track and have a horizontal resolution of ∼200–500 km along-track and a footprint of ∼3–9 km across-track. In this study we use version 4 (v4) Aura MLS N_2O, HNO_3, H_2O, HCl, ClO, and O_3 measurements from Arctic winters spanning 2004/05 through 2015/16. The quality of these data is described by Livesey et al. (2015a). Vertical resolution is about 2.5–3 km for O_3, 3 km for H_2O, HCl, and ClO, 3–5 km for HNO_3, and 5–6 km for N_2O in the lower to middle stratosphere, and about 5 km for CO in the middle stratosphere. Single-profile precisions are approximately 0.03–0.1 ppmv, 0.2–0.3 ppbv, 0.1 ppbv, 0.6 ppbv, 13–20 ppbv, and 16 ppbv for O_3, HCl, ClO, HNO_3, N_2O, and CO, respectively, and 5–15% for H_2O. The v4 MLS data are quality-screened as recommended by Livesey et al. (2015a). For daily maps, MLS data are gridded at 2°latitude by 5°longitude using a weighted average around each gridpoint of 24 hours of data centered at 12:00 UT.

Equivalent latitude (EqL, the latitude that encloses the same area between it and the pole as the corresponding potential vorticity, PV, contour, Butchart and Remsberg, 1986) and scaled PV ~~(sPV, scaled as in Dunkerton and Delisi, 1986; Manney et al., 1994)~~ (sPV, used in the analysis described below. These quantities, as well as temperatures from MERRA-2, are obtained at MLS locations from an updated version of the MLS derived meteorological products (DMPs) described by Manney et al. (2007). MLS data are interpolated to isentropic surfaces using temperatures from MERRA-2.

2.3 Vortex and temperature diagnostics

To investigate the potential for polar chemical processing and ozone loss during the 2015/16 winter, we use a standard set of polar processing diagnostics calculated from MERRA-2 data. We primarily make use of diagnostics described by Lawrence et al. (2015), including minimum temperatures~~(T_{min})~~, the volume of air with temperatures below polar stratospheric cloud (PSC) existence thresholds as a fraction of vortex volume (V_{PSC}/V_{Vort}), maximum PV gradients, and the area of the polar vortex in sunlight (or sunlit vortex area). All of these diagnostics are calculated from the 12:00 UT temperature and potential vorticity fields provided by MERRA-2 interpolated to isentropic surfaces between 390 and 580 K (approximately 120 to 30 hPa, or 14 to 24 km). In cases where a PSC temperature threshold is used to calculate a quantity, such as the area with temperatures below PSC thresholds (and the derived V_{PSC}), we also calculate the quantity using ±0.5 K offsets from the nominal PSC

thresholds to help quantify the sensitivity to the values used. Further discussion of these diagnostics and their significance to polar chemical processing can be found in Manney et al. (2011) and Lawrence et al. (2015).

Our analysis makes use of a detailed characterization of the 2015/16 stratospheric polar vortex, particularly during the period of time when the vortex split into multiple offspring. We use the CAVE-ART (Characterization and Analysis of Vortex Evolution using Algorithms for Region Tracking) analysis package, which was developed to comprehensively describe the state of the polar vortex throughout the winter season. A paper describing the full details and implementation of CAVE-ART is in preparation (Lawrence and Manney, 2016); in short, CAVE-ART uses image processing and region tracking algorithms to objectively identify any number of vortex regions and track their positions through time. CAVE-ART identifies vortex regions based on altitude-dependent contours of sPV that we specify as being representative of the vortex edge. These sPV values are selected using climatological profiles of sPV spanning 25 isentropic levels between 390 and 1800 K to identify the sPV value at each level that coincides best with maximum sPV gradients from the MERRA reanalysis. Once CAVE-ART identifies individual vortex regions, it filters out those below a specified area threshold; except where otherwise noted, we use herein an equivalent latitude threshold of 84°, which is an area of roughly 0.5% of a hemisphere. All remaining regions are then tracked through time using the full time resolution of the meteorological data (eight times per day for MERRA-2) until the regions fall below the area threshold, or in some cases merge with another region. CAVE-ART also calculates and saves diagnostics at every timestep that describe the position, size, and strength of each region. These diagnostics include 2-D moment diagnostics such as aspect ratios and centroids (e.g., Matthewman et al., 2009; Mitchell et al., 2011), vortex areas, average altitudes, and vortex-edge windspeeds.

Such detailed characterizations are particularly useful during vortex-split SSW events wherein the resulting offspring vortices can vary in size and strength in ways that ultimately influence polar processing. For example, a preliminary version of CAVE-ART was used by Manney et al. (2015a), to show how the early January 2013 vortex-split SSW was responsible for accelerated ozone loss in January 2013. For the current paper, the CAVE-ART characterization is particularly important because, as will be shown, during the 2016 MFW, the vortex rapidly weakened and briefly split into three offspring vortices at some levels. The capability to track more than two offspring vortices is, to our knowledge, currently unique to CAVE-ART, as other methods in the literature rely on moment diagnostics that can, at best, delineate between only two regions (Mitchell et al., 2011). We have included a supplementary animation that shows the evolution of the polar vortex during the March 2016 MFW, which illustrates the CAVE-ART characterization of the vortex split.

2.4 Transport and Mixing Diagnostics

EqL time series of MLS data are produced using a weighted average of MLS data in EqL and time, with data additionally weighted by measurement precision (e.g., Manney et al., 1999, 2007). All vortex averages of MLS data shown use the altitude-dependent sPV values derived for CAVE-ART to identify the edges of the vortex or vortices (Section 2.3). For averages in multiple vortices, the sPV from the MLS DMPs is first used to determine whether the MLS measurement location is within any vortex. Those points that are within a vortex are then marked with the labels for individual regions provided by CAVE-ART to identify which of multiple vortices they are inside. Vortex averages are shown here for "bulk" (all MLS measurements with

sPV greater than the altitude-dependent threshold), "sum" (the sum of all the regions with area greater than the 84°EqL cutoff used in the CAVE-ART runs), and for individual vortices identified by CAVE-ART. Averaging improves MLS precisions to values smaller by a factor of about 10 to more than 100 over the single-profile precisions listed in Section 2.2 for EqL gridded and vortex averaged fields..

sPV gradients and effective diffusivity (K_{eff}) as a function of EqL calculated from MERRA-2 PV are shown as "global" (that is, characterizing amounts averaged around EqL contours) diagnostics of mixing. Gradients of sPV as a function of EqL provide a measure of the strength of the vortex edge as a transport barrier averaged over each day and all vortices (Manney et al., 2011, 2015b, and references therein). K_{eff} is expressed as log-normalized equivalent length, i.e., the length of a tracer contour with respect to the contour of minimum length that would enclose the same area; high (low) values thus reflect complex (simple) structure in tracer (here PV) contours and indicate strong (weak) mixing (e.g., Nakamura, 1996; Haynes and Shuckburgh, 2000; Allen and Nakamura, 2001). The magnitudes of K_{eff} values depend strongly on the resolution of the PV fields used in the calculations, but K_{eff} distributions from MERRA-2 agree morphologically with those calculated from other analyses and reanalyses. Similarly to sPV gradients, the gradients of long-lived trace gases on isentropic surfaces as a function of EqL indicate the strength of the vortex edge transport barrier. We use the EqL/time gridded MLS fields to calculate these gradients.

The diagnostics of mixing and transport barriers described above represent averages around EqL contours, and thus give information on bulk mixing properties; for example, the strength of the transport barrier at the EqL of the vortex edge is an estimate of that barrier averaged over the ~~the~~ entire length of the edges of all vortices present at that time. To examine regional mixing (e.g., variations along the edge of a vortex, or differences between individual vortices), we use the function M (hereinafter referred to as M) to give a synoptic picture of the strength of the vortex transport barrier prior to, during, and after the 2016 MFW. M is a Lagrangian diagnostic (Madrid and Mancho, 2009; Mancho et al., 2013) calculated from parcel trajectories that has been used to highlight processes related to transport and mixing in geophysical fluid flows ~~(Mendoza and Mancho, 2010; de la Cámara et al., 2012; de la Cámara et al., 2013; Smith and McDonald, 2014)~~ (Mendoza and Mancho, 2
The formal definition of the function M is as follows: consider a point in an n-dimensional space defined at an initial time t_0 by the general coordinates $(x_{1,0},...,x_{n,0})$. If a parcel is initialized at this point and advected by the background velocity field ($\frac{dx_i}{dt}$), then the function M at this point is ~~then~~ defined by the integral equation $M(x_{1,0},...,x_{n,0},t_0) = \int_{t_0-\tau}^{t_0+\tau} \left[\sum_{i=1}^{n} \left(\frac{dx_i}{dt}\right)^2\right]^{1/2} dt$. This is the Euclidean arc length of the trajectory traced out by the parcel in the time interval $[t_0-\tau, t_0+\tau]$. If a grid of such points and parcels is constructed, then a field of M can be defined by calculating the above integral for each point, or initial condition, within the grid. Hence, M is a function that relates arc lengths of trajectories to their initial conditions in some specified domain (Madrid and Mancho, 2009) . For our application, we ~~instead~~ calculate a field of M by using zonal and meridional winds in a trajectory code to advect parcels initialized on a regular longitude/latitude grid. We then calculate M by summing up the distances between parcel locations at successive times assuming that these locations are connected by great circle arcs.

We use the core of the Lagrangian trajectory diagnostic code described by Livesey et al. (2015b) to calculate parcel advection using a fourth-order Runge Kutta scheme. The trajectories we use here are calculated via integrations with a fifteen minute timestep from MERRA-2 winds. We initialize parcels on a 1.25 ~~x~~ × 1.00 degree longitude/latitude grid (a grid ~~spacing twice~~

~~the size of the native grid~~ defined by downsampling MERRA-2's native grid by half in both longitude and latitude dimensions) poleward of 20°N. The calculations of M are based on isentropic trajectories that are carried out for 15 days forward and backward (i.e., $\tau = 15$ days, for 30 days total) from 00:00 UT on the initialization date.

M has been used before to study transport ~~in~~ and dynamics in and around Earth's polar vortices. de la Cámara et al. (2012) used M to define hyperbolic trajectories and invariant manifolds in the lower stratospheric flow of the southern hemisphere during the 2005 Southern spring, which helped to explain transport across the vortex edge. In a later study, de la Cámara et al. (2013) used M and reverse domain filling calculations of potential vorticity to diagnose signatures of Rossby wave breaking in the Antarctic polar vortex and explain the trajectories of isopycnic balloons launched as part of the Vorcore and Concordiasi field campaigns. Smith and McDonald (2014) used average values of M and the area of large M values to describe polar vortex strength and ~~the permeabilityof its edge~~vortex edge permeability. Even more recently, Guha et al. (2016) used M to identify hyperbolic trajectories associated with planetary wave breaking in a single-layer shallow-water model of the Austral spring stratosphere, and as a result, they were able to characterize the specific wave forcings required for wave breaking to occur inside and outside the stratospheric polar vortex. Although there ~~has been some recent debate on~~ is an ongoing discussion about the usefulness of M for describing flow characteristics (such as invariant manifolds and hyperbolic trajectories~~(see, e.g., Ruiz-Herrera, 2015; Balibrea-Iniesta et al., 2016)~~) in different scenarios (see, e.g., Ruiz-Herrera, 2015; Haller, 2015; Balibre here we use M in an arguably simpler manner similar to that of Smith and McDonald (2014); namely, large values of M indicate parcels that were effectively trapped in a transport barrier for most of the trajectory timeline, whereas small values of M indicate the opposite with parcels that were more prone to ~~mixing. We also use~~ stirring/mixing. This might be too simplistic of an assumption for some cases, but in the context of the stratospheric polar vortex, the dominant flow features are defined by the polar night jet acting as a mostly impermeable barrier between the surf zone and intra-vortex air, which are regions where we can reasonably assume air is not advected to the same great extent as within the vortex edge. Part of our analysis with M uses an area diagnostic similar to that ~~in~~ from Smith and McDonald (2014), obtained by calculating the area enclosed by contours of M for the entire grid, and expressing these as an equivalent latitude, which we denote by "M-EqL". Although EqL is most commonly used to describe the area within PV or tracer contours (e.g., Butchart and Remsberg, 1986; Allen and Nakamura, 2003) (as PV-based EqL is used herein), we have found that examining M and M-EqL together facilitates understanding of how the size, strength, and sharpness of the vortex edge transport barrier evolve with time.

~~We also~~ The following list briefly summarizes the diagnostics of transport barriers and mixing used here:

- **PV gradients** Gradients of scaled PV as a function of EqL reveal the EqL location and sharpness of the vortex edge because PV increases dramatically between the surf zone and the vortex interior.
- **K_{eff}:** Effective diffusivity (K_{eff}) measures the geometric complexity of tracer (herein PV) contours, and is thus a proxy for mixing.
- **The function M:** This function corresponds to the distance traveled by parcels advected by the background flow over a specified time interval, which helps quantify the permeability of the vortex edge and the degree of separation between intra- and extra-vortex air.

– **Trace Gas Gradients:** Trace gases measured by MLS, such as N_2O, CO, and O_3 have strong gradients across the vortex edge due to confined descent, and thus their gradients help identify the EqL location and sharpness of the vortex edge transport barrier.

In addition to identifying transport barriers and mixing regions as described above, we use the trajectories described above for the calculation of M to explore the origins and fate of air from the polar vortex during its breakup. We use the CAVE-ART identification of vortex regions to "tag" parcels that were initialized inside each valid and distinct vortex region. This allows us to examine the full history of parcels with respect to their original confinement within materially separated vortex regions. Similar trajectories were ~~calculated using the~~ also calculated using full 3D ~~trajectory code with diabatic motions, and~~ advection with diabatic heating rates, but only extending backwards from 12:00 UT each day, for use in reverse domain filling (RDF) calculations initialized with MLS data; the MLS fields used for these initializations are the gridded map fields described above.

3 Overview of 2015/16 Polar Vortex Evolution and Composition

Figure 1 gives an overview of dynamical conditions in the Arctic lower stratosphere during the 1979/1980 through 2015/16 winters using the polar processing diagnostics ~~calculated from as described above (~~described in Section 2.3 ~~)~~calculated from MERRA-2. Figure 2, which shows vortex-averaged (summed over all vortices identified by CAVE-ART) trace gases in the lower stratosphere from Aura MLS data for 2004/05 through 2015/~~16. The period of the Aura mission~~ 16, illustrates the consequences for polar chemical processing of the meteorological conditions shown in Figure 1. The Aura mission period has included numerous winters with conditions at the extremes of Arctic variability, in both meteorology and chemical composition~~:~~ ; comparison with these earlier extreme Arctic winters provides context for the vortex evolution and associated polar processing in the 2015/2016 winter.

The 2010/11 winter ~~was not overall~~ (blue lines) was not in general characterized by record low temperatures, but rather by an exceptionally prolonged period, extending into early April, of temperatures ~~low enough to activate chlorine~~ below the chlorine activation threshold (Figure 1a~~,b, Figure 2d,e)~~), and an unusually strong and persistent lower stratospheric vortex (Figure 1~~e~~b). As a result, chlorine activation persisted later than observed in any other Arctic winter (Figure 2d,e) (Manney et al., 2011; WMO, 2014, and references therein). These conditions enabled unprecedented ozone loss (Figure 2f); in fact, the vortex remained strong and relatively cold after the period shown here, and ozone continued to drop, reaching a minimum of ~1.5 ppmv in late April (e.g. Manney et al., 2011; WMO, 2014). While the vortex was exceptionally strong and vortex-averaged ozone loss unprecedented in the 2010/11 winter/spring, the size of the vortex during much of ~~the~~ that winter (through late February), and the portion of it exposed to sunlight, were both less than average (Figure 1~~d~~c).

In early January 2013 (orange lines), temperatures abruptly rose far above ~~those at which chlorine can be activated (and hence chemical ozone loss occur) during one of the strongest~~ the chlorine activation threshold during a "vortex-split" SSW. This event was among the strongest SSWs on record~~(Manney et al., 2015a) ; however~~, with one of the largest abrupt temperature increases, deepest vertical ranges of wind reversal, and most prolonged periods of easterlies. However, the exceptional cold prior to that event (Figure ~~1a,b~~1a), and exceptional exposure of the vortex ~~(offspring vortices)~~ and offspring vortices to sunlight in Decem-

ber ~~(January)~~ and January (Figure 1~~d~~c) led to denitrification comparable to that in 2011 (Figure 2b) and the largest early winter chlorine activation and ozone loss on record ~~(Figure 2d,e,f) (Manney et al., 2015a)~~ (Figure 2d,e,f; Manney et al., 2015a) .

The meteorological conditions in 2014/15 ~~provided a counterexample, where a very~~ (green lines) led to the opposite extreme of polar processing. A brief minor SSW split the vortex on 5 January 2015, after which temperatures ~~quickly~~ soon dropped below the chlorine activation threshold again~~, led to~~ . The resultant rapid chlorine deactivation~~and~~, combined with exceptionally strong descent within the vortex (as seen in the record N_2O/H_2O decrease/increase, Figure 2a,c)~~(Manney et al., 2015b) ,~~ , led to the highest January/February ozone values in the MLS record (Figure 2f; Manney et al., 2015b) .

In comparison to these previous recent years with exceptional combinations of dynamical conditions leading to unanticipated extremes in Arctic polar processing, the 2015/16 winter (red lines) stands out as yet another unexpected extreme in variability of the Arctic winter stratosphere. Minimum temperatures (Figure 1a) were well below average from late November through mid-March, and near or at record lows from late December ~~though~~ through January. The period of over a month, from late December through early February, with temperatures below the approximate ice PSC threshold was unprecedented ~~in~~ for the Arctic, where the ~~previous~~ MERRA-2 record rarely shows more than a few contiguous days below this threshold~~and never more than~~ ; unusually long periods of about three weeks with temperatures below the ice PSC threshold did, however, occur previously in 2010 (Manney et al., 2015a, and references therein) and 2011 (Figure 1a~~and Figure 3c,d~~). The long period of temperatures below the ice PSC threshold led to ~~a much greater degree of dehydration than has been seen before~~ much greater dehydration than previously seen in the Arctic: Compare the evolution of H_2O in 2016 in Figure 2c with the small decrease in H_2O seen in 2011 when there were separated periods in late January and February of about one and three weeks' duration, respectively, with temperatures below the ice PSC threshold. The presence of large ice PSCs ~~also can~~ can also lead to greater denitrification than the presence of (typically smaller) NAT or liquid PSC particles alone (e.g., Wofsy et al., 1990; Hintsa et al., 1998; Santee et al., 1998; Lowe and MacKenzie, 2008; Dörnbrack et al., 2012; Wohltmann et al., 2013), and is consistent with the extreme denitrification evident in Figure 2b. Figure 1~~d~~ c shows that the 2015/16 vortex was not only larger than usual, but also had a larger area than usual receiving sunlight during January through mid-March.

The exceptionally cold conditions resulted in extensive early winter chlorine activation in 2015/16, with low HCl values in late December/early January matched only by those in 2012/13 (Figure 2d). Greater than usual sunlight exposure also resulted in high ClO (Figure 2e), with values in January through mid-February higher than those in 2011. Because of this extensive chlorine activation, chemical ozone loss began early, with a downward trend in vortex-averaged ozone (Figure 2f) seen beginning at the end of December 2015. Only in 2012/13, with exceptional cold and sunlight exposure in December ~~(Figure 1a,d; Manney et al., 2015a)~~ (Figure 1a,c; Manney et al., 2015a) , did ozone begin decreasing earlier. The onset of an observed ozone decrease means that chemical loss had become large enough to dominate over replenishment by descent of air within the vortex~~;~~ . Figure 2a shows that early winter descent was similar in ~~2015/16, 2012/13, and 2010/11:~~ all four years highlighted; thus the relative timing of the start of the ozone decrease reflects that of the onset of chemical loss.

Ozone continued to decrease in the vortex at a rate slightly faster than that in 2011 until the beginning of March 2016. If uninterrupted, ozone values would have been expected to drop lower than those in 2011 by mid-March. Instead, before mid-March, a brief increase of about 0.5 ppmv was followed by about a week of decreasing values and then slightly increasing

values for the rest of the winter (Figure 2f). ~~(~~, resulting in observed ozone values always remaining higher than those in 2011. At lower altitudes, near 430 K ~~, not shown~~(not shown), vortex averaged ozone in 2016 was up to ∼0.2 ppmv lower than that in 2011 from late January until early March when the MFW began, but then rapidly rose above 2011 values. ~~) Figures~~Figure 1a ~~and b show~~ shows that temperatures rose above the activation threshold by mid-March, and Figures 1~~c and d~~ b and c show a sudden decrease in vortex strength and area just before mid-March, with the vortex being nearly gone by mid-April. Furthermore, N_2O values (Figure 2a), which had been decreasing steadily via descent in the vortex, rose suddenly by about 20 ppbv around the time of the vortex split (second red vertical line), subsequently dropped again by over 20 ppbv, then remained highly variable with little trend for the rest of the winter. The return of ClO values to near-zero was concurrent with the beginning of the final upturn in ~~ozone in the vortex~~ vortex ozone (Figures 2e,f). Temperatures began rising and ClO decreasing in the last week of February, with minimum temperatures exceeding the activation threshold just before the vortex split (Figure 1a). The steep decrease in ClO began nearly a month earlier than that in 2011.

V_{NAT}/V_{Vort} (V_{PSC}/V_{Vort} calculated for nitric acid trihydrate PSCs and ~~integrated~~ averaged over a winter) is a diagnostic commonly used to indicate the overall potential for polar processing and ozone loss (e.g., Rex et al., 2004; Tilmes et al., 2006). The polar processing potential in 2015/16 estimated using this diagnostic (Figure 3a) was nearly identical to that in 2010/11. ~~Another measure, the number of days integrated over the lower stratosphere on which activation can occur (Figure 3b; e.g., Manney et al., 2011, Supplementary Information) shows values similar to the largest previously observed excepting 2011. Similar diagnostics~~ A similar diagnostic for the volume ~~and duration~~ of air below the ice PSC threshold (Figure 3~~c,d) indicate~~ b) indicates much greater potential for dehydration (and denitrification) than in any previously observed Arctic winter, even when accounting for the sensitivity of the calculations to the exact temperature used for the ice PSC threshold. It may be argued that more extensive denitrification in 2015/16 enhanced the ozone loss potential because of its effect of slowing chlorine deactivation (e.g., Douglass et al., 1995; Santee et al., 1996, 2008; Waibel et al., 1999; Davies et al., 2002). Thus, the critical factor resulting in less ozone loss than in 2011 was the much earlier increase in temperatures and vortex breakup in 2016.

Figure 4 shows the vertical extent of polar processing and the progression of the vortex breakup in 2015/16. The downward tilt of N_2O contours in Figure 4 until early March indicates very regular descent within the vortex, as does the downward progression of H_2O and O_3 contours above about 600 K where those species are not affected by lower stratospheric chemical processing. Increases in N_2O throughout the domain, and in O_3 above ∼600 K, after the MFW began suggest increased mixing into the vortex. The disappearance of significant vortex regions is marked by blank regions, and occurs in late March at and above about 850 K (in the middle stratosphere), early April down to about 500 K, and after mid-April at levels below that.

In contrast to 2011 and 2013, during which evidence of renitrification was seen above 400 K (e.g., Sinnhuber et al., 2011; Arnone et al., 2012; Manney et al., 2015a, b), sequestration in PSCs and denitrification led to depleted gas phase HNO_3 (Figure 4b) extending below 400 K in 2015/16. Sequestration in ice PSCs, and evidence of dehydration (in that low vortex H_2O lingered well beyond the period with temperatures below the ice PSC threshold) is apparent in Figure 4c from about 420 K to above 550 K. Extensive chlorine activation is apparent from about 400 K up to above 600 K (Figure 4d,e), an upper extent comparable to that in the Antarctic. The upward tilt of ozone contours (Figure 4f) at levels from below 400 K to above 600 K

beginning in early January indicates sufficient chemical ozone loss to exceed the replenishment by descent. This signature extends until mid-February at the higher levels, early March near 500 K, and continues into April at the lowest levels shown.

In the following, we focus on the evolution of the vortex and trace gas transport during the MFW on the individual isentropic surfaces marked by horizontal lines in Figure 4. 850 K (∼31 km, estimated from CAVE-ART vortex averaged altitude over the winter) is shown to represent the middle-stratospheric regime where the vortex decay is very rapid. 490 and 550 K (∼20 km and 22 km, respectively) represent the two regimes in the lower stratosphere with significantly differing vortex evolution during the MFW. These lower stratospheric levels are near the maximum (490 K) and top (550 K) of the region of chemical processing. As seen in Figure 4, both of these lower stratospheric levels had exceptional chemical processing and large ozone loss by early March 2016.

4 The 2015/16 Major Final Warming: Vortex Breakup and Mixing

4.1 Overview of transport barrier and trace gas evolution

~~Timeseries~~ In Figures 5–7 we show timeseries of sPV gradients, K_{eff}, and MLS trace gases ~~(Figures 5–7) as a function of EqL~~ as functions of EqL at 850, 490, and 550 K to contrast the evolution of trace gases in the middle stratosphere with that in the lower stratosphere, and to compare the evolution at two lower stratospheric levels where significant polar processing took place. These diagnostics provide an overview of the vortex and chemical evolution throughout the 2015/16 winter.

In the middle stratosphere at 850 K (Figure 5), sPV gradients and K_{eff} indicate a consistently strong transport barrier along the vortex edge (strong maximum/minimum in sPV gradients/K_{eff}) through early March. The vortex area shrinks steadily through the winter, even as the vortex edge transport barrier strengthens and mixing outside the vortex increases (weaker sPV gradients, higher K_{eff}). This is consistent with the climatological development of the Aleutian anticyclone, intensified mixing in the surf zone, decreasing vortex area, and accompanying strengthening of PV and tracer gradients along the vortex edge (e.g., McIntyre and Palmer, 1984; Leovy et al., 1985; Butchart and Remsberg, 1986; Harvey et al., 2002). Lower sPV gradients and higher K_{eff} at midlatitudes in February indicate increasing activity in the surf zone (as has been previously reported, e.g., Haynes and Shuckburgh, 2000; Allen and Nakamura, 2002) consistent with the spreading of higher H_2O values out from the vortex edge region. CO, because of its extremely strong gradients across the vortex edge, provides a sensitive indicator of export of vortex air, and indicates periods of such enhanced transport in mid-February and early to mid-March. After the MFW began, the rate of vortex shrinkage accelerated rapidly, with the area enclosed within a transport barrier (sPV gradient maximum, K_{eff} minimum) approaching zero by the end of March. The H_2O and CO values show only slightly weakened gradients across the vortex edge in its final days, suggesting that most of the air in the remnants of the vortex was well confined within them until they disappeared.

In the lower stratosphere, at 490 K (Figure 6) the maximum PV gradients align closely with the minimum in K_{eff} and indicate a strong barrier to mixing. The large and strong vortex persists until nearly mid-March, past the start date of the MFW. In early February, maximum K_{eff} in mid-latitudes increases, suggesting that more vigorous mixing in the surf zone extends down into the lower stratosphere (consistent with the results of, e.g., Waugh and Randel, 1999; Harvey et al., 2002). Vortex area suddenly

decreased and maximum sPV gradients/minimum K_{eff} decreased/increased immediately after two small offspring split off the vortex (around 13 March, second vertical red line), leaving the larger parent vortex even more distorted (see supplementary animation).

The signatures of mixing vary between trace gases depending on region and times because of differing horizontal gradients. Evidence of air from near the vortex edge mixing out into midlatitudes is seen in N_2O, H_2O, and O_3 during February in the spreading of values previously characteristic of the vortex edge throughout the midlatitude surf zone. ~~This is consistent with the common pattern of filaments of air being drawn off the vortex, around and into the anticyclone during this period. HCl shows consistent~~ HCl shows evidence of some mixing of very low values out of the vortex, with ~~a concurrent extrusion~~ concurrent extrusions of high ClO, in early February; these signatures are short-lived, since active chlorine transported out of the vortex in filaments rapidly decays via both deactivation and mixing ~~(e.g., Konopka et al., 2003; Tan et al., 1998; Marchand et al., 2004) . Additional brief events of this sort are seen in mid-February and mid-March, and evidence of this mixing out of the vortex is also apparent in HNOand H~~(e.g., Tan et al., 1998; Konopka et al., 2003; Marchand et al., 2004) . Small increases in vortex N_2O and O_3 (just inside the overlaid sPV contours in the region of strong gradients) concurrent with the split suggest some mixing of extra-vortex air into the vortex region associated with that event, but the largest change following the split is the decrease in extra-vortex N_2O and O_3 values, suggesting vortex erosion is the dominant process. Similar evidence of increased mixing into midlatitudes after the vortex split is apparent in H_2O and HNO_3.

At this level, minimum temperatures rose above the ice PSC threshold in late February, and the steady increase in H_2O after that time indicates evaporation of ice PSCs. Minimum temperatures exceeded the chlorine activation threshold on about 13 March, nearly concurrent with splitting of the vortex (see Section 2.4). The evolution of HCl and ClO indicate rapid deactivation at this time, though non-zero ClO values lingered in the vortex until its disappearance in mid-April. Once chlorine is largely deactivated (after mid-March in 2016), very high HCl values in the vortex make it a good tracer of transport (e.g., Manney et al., 2005), and substantial mixing into midlatitudes is apparent, consistent with the signature in the other species.

While the transport barriers seen in sPV gradients and K_{eff} are weaker after mid-March, a significant maximum and minimum, respectively, remain along the edge of the rapidly shrinking vortex through early April. It is only at this time (apparent around 7 April in Figure 6) that very low N_2O and O_3 previously confined to the vortex core are seen equatorward (in EqL) of the strong PV gradients, indicating the final decay of the vortex.

A somewhat similar evolution is seen at 550 K (Figure 7), with a large vortex bounded by a strong transport barrier into early March, accompanied by increased mixing in midlatitudes in February consistent with filamentation and a more vigorous surf zone. In contrast to 490 K, ~~however,~~ while the vortex area ~~shrinks~~ shrank after the onset of the MFW and vortex split, the maximum sPV gradients remained about as strong as before the split, and K_{eff} continued to show a more pronounced minimum than at 490 K. ~~Consistently~~Consistent with these indications of a persistent strong transport barrier, N_2O and O_3 (and other trace gases, not shown) ~~do not suggest substantial~~ gradients near the vortex edge remained stronger than those at 490 K, with less spreading of low N_2O and ozone values out from the vortex edge, indicating more limited mixing out of the vortex core ~~until~~ through mid-April. Note that, similar to 490 K, vortex ozone was also strongly depleted at this level, resulting in very

strong gradients along the inner edge of the vortex. At this level, however, the unperturbed morphology of ozone is such that vortex values are generally much lower than those outside the vortex prior to the onset of chemical loss.

~~The~~ Figure 8 shows the evolution of transport barriers and trace gases in ~~the lower stratosphere is examined in more detailin Figure 8. Figure 8 compares~~ more detail, comparing the sPV gradients and K_{eff} on each day during the period surrounding the MFW with the evolution of ~~M,~~ N_2O ~~gradients,~~ and O_3 gradients and M as a function of EqL, as well as the evolution of M as a function of "M-EqL" (see Section 2.4). The period ~~covered is from~~ spans 24 February, about 10 days before the beginning of the MFW, through 15 April, when the vortex was disappearing. The transport barriers shown by sPV gradient and M maxima, K_{eff} ~~and M~~ minima, and strongest trace gas gradients are all closely aligned. The vortex edge transport barrier was near 65°EqL through the time of the vortex split, after which it shifted to about 75°EqL, indicating a substantial decrease in the total vortex area. The ozone gradients show a "dipole" pattern, with a large positive extrema near 60°EqL switching to a large negative one just poleward of it – this is the signature of increasing values in the outer vortex edge region changing to rapidly decreasing values moving into the vortex core where extensive chemical ozone loss has occurred. Note that on a given day the values of M do not fall off as sharply on the high-EqL side of the peak as do those of sPV gradients and K_{eff}. This is primarily because M values at EqLs higher than that of the vortex edge represent parcels that have, over the period of the calculation, been largely confined within the polar vortex, where they are likely to have spent some time near the edge in the region of high winds (thus travelling relatively long distances on average); conversely, the parcels at EqLs outside the vortex are largely in the surf zone where winds are weak and parcels do not linger near the vortex edge. The extrema of gradients in N_2O and O_3 correspond well with those of the ~~mixing~~ other diagnostics: The EqLs of the strongest negative N_2O gradients closely matched those of the mixing diagnostics, while the largest negative gradients in O_3 were located around 5°EqL poleward of that, consistent with their origin along the edge of the strongly ozone-depleted vortex core. The transport barrier presented by the vortex edge at this level rapidly weakened and moved poleward of 70°EqL shortly after the split, and continued this progression through the end of March. In early April, a weak transport barrier was still apparent just equatorward of 80°EqL, as reflected in the trace gas gradients. The location of the strongest O_3 gradient was aligned with the extrema in ~~mixing~~ the other diagnostics on this date, suggesting that the remaining vortex had largely been "stripped down" to its original core region. A similar pattern of evolution was seen at 550 K, and close alignment of transport/mixing diagnostics and trace gas gradients was seen through the middle stratosphere (not shown).

Binning M as a function of M-EqL is a convenient way of combining the size and strength of the polar vortex into a single diagnostic. Although M is not a tracer (or tracer-like field), calculating EqL from any field provides an intuitive way of examining the area enclosed by its contours. We have found that plotting M as a function of M-EqL is an easy way of showing the maximum distance traveled by a single parcel (at 90° M-EqL), which acts as a proxy for the strength of the vortex edge region over the 30 day trajectory period. If the vortex edge is strong and relatively wide, M as a function of M-EqL will flatten towards the maximum value, indicating that a sizable fraction of parcels ended up "trapped" by the strong winds within the vortex edge and thus traveled long distances. While the slopes of the lines in late February and the first few days of March show this "flattened" shape above about 70° M-EqL, after the MFW starts, these move in toward 80° M-EqL, indicating that many fewer parcels ended up within the vortex edge region as the vortex weakened and decayed. Starting shortly after the vortex

split, the flattened area virtually disappears, indicating a very small and/or weak transport barrier. Furthermore, the maximum M value decreases on average by 1.51 Mm per day throughout the period, which shows the rapidity of the weakening of the vortex edge transport barrier. That the flattened ~~area~~ shape mentioned above disappears while M values still show a pronounced upward slope towards 90° M-EqL is consistent with the changes in the locations of extrema in the trace gas gradients and the picture of very small vortex areas lingering that were bounded by a significant transport barrier.

The EqL-based view presented above gives a global perspective on the evolution in vortex area and strength during the MFW period. This averaged view of transport barrier and mixing diagnostics shows that a small area of well-confined vortex air lingered through March, but by early April the transport barrier presented by the vortex edge was greatly weakened, and the potential for mixing was high. In the following, we focus on the synoptic evolution of the vortices and regional aspects of transport and mixing during the MFW period.

4.2 Synoptic evolution, vortex splitting, and local mixing

Figure 9 shows maps of MLS CO and H_2O~~and~~, as well as M, in the middle stratosphere at 850 K, along with scatterplots of M versus sPV for dates near the beginning of the MFW (7 March), near the time of the vortex split (13 March), as the offspring are shrinking (19 March), and just before the last offspring vortex disappears (4 April). In early March, the polar vortex at this level was much smaller than earlier in winter (as seen in Figure 5), and was elongated and shifted far off the pole as is typical of a displacement SSW (Charlton and Polvani, 2007). A long filamentary tail was drawn off the main vortex and around the Aleutian anticyclone (whose "eye" can clearly be seen in M just north of Alaska on 7 and 13 March, in the same region as anomalously low water). A single offspring eventually split off the parent vortex near mid-March, and both vortex regions quickly weakened thereafter. Strong confinement is indicated in the maps of CO and H_2O throughout the period; even in early April when the polar vortex has almost completely decayed, elevated CO and H_2O signatures are seen in the remaining small vortex remnants. The maps of M show features consistent with the trace gases and vortex edge region, as well as enhanced M values in the anticyclone (along its edge, and spiraling into it). The high M values here indicate that the strong anticyclone acts as a transport barrier to trap air, and the spiral structure of the high values is consistent with tongues of air drawn off the vortex spiraling together with low latitude air forming persistent filamentary structures with very long transverse scales, as has been previously reported (e.g., Sutton et al., 1994). ~~Consistent with the entrapment of air for many days at this time, ozone reached very low values within the anticyclone, forming a "low-ozone pocket" (e.g. Manney et al., 1995; Harvey et al., 2004) (not shown).~~ The scatterplots of M versus sPV initially show a "horseshoe" pattern that indicates the range of sPV values comprising the vortex edge region; that is, M values show a relatively broad maximum in the vortex edge where parcels travel the furthest, though the picture is somewhat "blurred" by the high M values associated with the anticyclone, which is associated with very low PV, but still acts to coherently and rapidly transport air over long distances and thus gives enhanced values of M. The vertical red lines indicate the contour chosen to define the vortex edge in CAVE-ART, and show that this contour is near the maximum in M as long as the horseshoe shape ~~(indicating a significant transport barrier exists)~~ is well defined; this indicates that the sPV contour used to define the vortex edge is well within the range of sPV values in the transport barrier (strong gradient) region. The vortex/vortices weakened very quickly at this level, and the horseshoe pattern rapidly disappeared. An animation of the

M versus sPV scatterplots over the 24 February–15 April period is given in the supplementary information and shows this evolution in more detail.

Figures 10 and 11 show similar maps in the lower stratosphere, but with MLS N_2O and O_3. At 490 K the vortex shrank rapidly between 7 and 13 March preceding a brief triple split after 13 March (nearly simultaneous with the split at 850 K, consistent with the barotropic structure of "split" SSWs, e.g., Matthewman et al., 2009). Of the three resulting vortices, the largest and most stationary (referred to below as the "parent") vortex over Siberia stayed the strongest and most coherent. ~~The offspring~~ Air within the offspring vortex that formed over Greenland/Canada was ~~also relatively strong~~ initially well-confined, as indicated by the low N_2O and O_3 values on 13~~and 19 March. In contrast, the offspring over Europe was much more transient and subject to significant mixing, indicated by higher~~ March, but this vortex was sheared out and dissipating by 19 March; this is termed "offspring-s" (for short-lived) below. N_2O and O_3 values ~~than in the parent and stronger offspring vortices~~on 13 March were higher in the offspring vortex over Europe than the other vortices, indicating significant erosion at the time of the split; however, this offspring vortex ("offspring-p", for "persistent") remained coherent longer and moved over Greenland/Canada by 19 March. The maps of M show qualitatively the same picture, with the largest M values occurring in the edge region of the Siberian vortex. Large M values also occurred in the edge regions of the smaller offspring vortices on and shortly after 13 March, but decreased quickly thereafter as those vortices weakened and disappeared. Note that values of M vary along the edge of a vortex in a manner that appears consistent with the trace gas gradients – for example, a region of very high M values crossing near the pole north of Alaska on 7 March was associated with particularly strong gradients in N_2O and O_3. Small differences in the shape of the vortex edge sPV contour and the maximum M region reflect the fact that M is calculated from 30 days of information during a period of rapid change in the vortex. Scatterplots of M versus sPV show ~~strong~~ distinct horseshoe patterns that indicate the range of sPV values comprising the vortex edge region, and again indicate the appropriateness of the choice of vortex-edge sPV contour. As the vortex/vortices weakened, this horseshoe pattern became less well-defined, indicating the degradation of the transport barrier and increase in mixing; this process was slower in the lower stratosphere than in the middle stratosphere, consistent with the slower vortex break down. (Also see the animation of the M versus sPV scatterplots given in the supplementary information.)

At 550 K (Figure 11) conditions were fairly similar, but the vortex split ~~into only two offspring~~ only in two (according to our vortex-edge definition), with ~~the Siberian vortex region~~ an initially larger and stronger ~~. Both offspring~~ parent vortex over Siberia, and a persistent offspring (again termed "offspring-p" below). Both vortices shrank rapidly in this period, but the MLS maps show that air was comparably well confined in each at the same time. The ~~smaller offspring~~ offspring-p vortex (corresponding to the ~~offspring over Greenland/Canada~~ more persistent offspring vortex at 490 K ~~) in particular~~ that moved over Greenland/Canada) was much stronger at 550 K than at 490 K. This is indicated by the MLS trace gases showing significantly larger regions with trapped low N_2O and O_3 depleted air all the way out through 4 April. This is also reflected in the maps of M, which show comparable values in the edge regions of both parent and offspring into early April. The offspring-p vortex shows a small "hole" in its center in early April where sPV drops slightly below the value used to identify the vortex edge; this does not appear to be significant for transport/mixing, since it is not associated with a noticeable increase in M values. Scatterplots of M versus sPV also show horseshoe patterns that are similar to, but more pronounced than, those seen at 490 K.

Even in early April as both parent and offspring start to decay, a horseshoe pattern is apparent with a double "arch" structure showing the distinctly different strength of the two ~~(both quite persistent) offspring~~vortices; this double arch is apparent from 30 March and through 7 April (see supplementary animation). As was the case at 850 and 490 K, the vortex-edge sPV contour lies near the maximum in M. Note, however, that there is a well-defined region of relatively high M seen in the map, and apparent in a local maximum in the horseshoe at lower sPV, on 13 March. There are also corresponding regions of low values in the MLS N_2O and O_3 maps. Examination of daily maps (not shown) indicates that this was a coherent fragment of air from the vortex edge region that had sPV just below the threshold used by CAVE-ART, and this remnant persisted through about 18 March – this represents the upward extension of the ~~third offspring~~ offspring-s vortex seen at 490 K.

~~Figure ?? shows~~ The trajectory-based air parcel history maps ~~at 850K initialized on 12 March, just before the vortex split described above. On this date (column 2), a long filament of significant area had been drawn off the vortex and broken up into two pieces, each large enough to be identified in as a vortex region. Though these were drawn off the vortex edge on 12 March, that air had been deep within the vortex 14 days before (column 1); this indicates that there was substantial mixing within the vortex itself. After being drawn off, these narrow filaments quickly dissolved, with the air from them being widely dispersed through the hemisphere by 20 March (column 3) and even more randomized by 26 March (column 4). After splitting in two on 14 March, the air from the narrow elongated offspring vortex suffered a similar fate to those in these filaments and was quickly dispersed, while the other small offspring survived into early April (not shown). The rapidity of the dispersal of air shown here is consistent with the picture of the very rapid vortex break up in the middle stratosphereshown above in Figures 5 and 9.~~

in Figures 12 and 13 show further details of the vortex evolution in the lower stratosphere. Figure 12 shows ~~similar~~ air parcel history maps at 490 K ~~during and~~ initialized after the vortex split. The air parcels in the vortices on 16 March (about two days after the split, row A) originated within the vortex 12 days earlier, with the parcels in the two small offspring vortices (~~green and blue~~blue and green for offspring-s and offspring-p, respectively) coming primarily from the narrower portion extending south near 30°E longitude. After the split, most of the air in the ~~blue offspring~~ green offspring-p vortex, which originated near 0° longitude, remained within a tight confined region for over two weeks, even after a vortex was no longer identified in that region. The 20 March initialization (row B, column 2) ~~, in which the blue vortex is the same one as the more persistent vortex region from the 16 March initialization, shows that this offspring~~ shows that the offspring-p vortex retained its identity into early April. The parent vortex (black) began to experience substantial filamentation in late March (row B, ~~column~~columns 3 and 4). This main vortex was ~~very small and had weakened~~ shrinking and weakening by early April (row B, column 4), but was still identified as a vortex region ~~on~~ through 10 April ~~(row C, column 2)~~ and maintained some coherence into late April (~~row C, columns 3 and 4~~not shown).

At 550 K (Figure 13), the air parcels in the ~~smaller (green) offspring~~ green (offspring-p) vortex just after the split (row A) originated 12 days before primarily from a ring of air just inside the vortex edge. Most of the air in this ~~offspring~~ offspring-p vortex remained coherent through March (row A, columns 3 and 4; row B, columns 2 and 3). Another ~~small and very short-lived (~~transient (persisting only about a day) ~~offspring~~ vortex that broke off the parent on 24 March (row B, column 2, ~~blue~~ purple vortex) was rapidly sheared out and the air originating in it wrapped around the outside of the parent (black) vortex on 8 April (row B, column 4). By this time the air in the green ~~offspring~~ offspring-p vortex was starting to ~~lose its coherence, though it~~

~~can be seen (row C) that the~~ mix out, though most of that air remained within a relatively confined region through ~~15 April (row C, column 3) and still showed some coherence on~~ 20 ~~April (row C, column 4~~April (not shown).

~~Thus, compared to the rapid and wide dispersal of vortex air in the middle stratosphere, air~~ Air from even small offspring vortices in the lower stratosphere ~~maintained some coherence much longer~~ thus remained in distinct confined regions long after the vortex split in the lower stratosphere. At all levels, examination of the grey parcels – that is, all the parcels that were outside any vortex on the initialization day – without the overlaid vortex parcels indicates that few of them ~~move into coherent~~ were entrained into vortex regions. ~~That is~~Thus, as long as the regions were large enough to be identified ~~in~~ as vortices by CAVE-ART, they remained mostly devoid of air with extravortex origins. This indicates that the mixing during the vortex break up was largely one-way, with air mixing out of the vortices through filamentation as they eroded and lost their identity. This result is consistent with previous studies of dispersal of air from the lower stratospheric vortex (e.g., Chen et al., 1994; Manney et al., 1994), and with the picture of a shrinking and weakening vortex decaying primarily by erosion into midlatitudes.

Figure 14 summarizes how the transport and mixing processes described above affected trace gases in the lower stratospheric ~~vortex~~vortices. The top panels show the evolution of the vortex areas, and the MLS sampling of those vortices. An abrupt decrease in vortex area immediately followed the vortex split, with the total (sum of all vortices) area decreasing by about 40% and 30% at 490 and 550 K, respectively. This is consistent with the maps shown above and the time evolution shown in the supplementary vortex regions animation. At 490 K, the vortex size decreased more ~~slowly, but steadily,~~ gradually thereafter, to about 3% of the hemisphere by the end of March, and less than 1% of the hemisphere by mid-April. At 550 K, the decay was more step-like, with another fairly rapid decrease in the area to ~~a total of~~ about 3% of the hemisphere in late March~~(near the time the second (blue) small, but very short-lived,)~~, corresponding to the time when the very transient small offspring was pulled off and dispersed ~~),~~ (first purple points here, corresponding to purple region in Figure 13 row B); this was followed by a sudden disappearance of any vortex (that is, no vortex had area greater than about 0.5% of the hemisphere) by 12 April.

The MLS sampling of the large, strong parent vortex in January through mid-February included 500–700 measurements per day, but both its area and the number of measurements in it had dropped somewhat at all levels by 24 February (the start date of the panels in Figure 14). In general, the number of MLS measurements in the vortices closely tracks their area, and there are several MLS measurements in each: For every vortex region identified by CAVE-ART that lasted more than one day, the minimum number of MLS measurements on a day was at least six. This suggests that MLS usually provided relatively unbiased sampling of even small offspring vortices that were just larger than the 84°EqL cutoff used by CAVE-ART. The number of MLS measurements begins dropping earlier, in the period between the beginning of the MFW and the split, because the vortex shifted farther off the pole to where MLS sampling is less dense. The rate of decrease in MLS measurements in the vortex at 550 K was steeper before the split than at 490 K, consistent with the vortex at that level being shifted farther out into midlatitudes. At 490 K, the steepest decrease in vortex MLS measurements was right around the split date. The minimum in number of MLS measurements shortly after the split (especially apparent at 490 K) is likely related to the fact that the vortex was shifted very far off the pole into midlatitudes and moved closer to the pole, into areas more densely sampled by MLS, in the following several days (see, e.g., Figures 10 and 11).

Vortex edge windspeeds show a deep minimum in the period between the start of the MFW and the split. Windspeeds showed some day-to-day variability after the split, but ~~over all~~ overall decreased steadily. The minimum just prior to the split arises largely because the vortex had already developed into ~~two separate~~ multiple closed circulations that were only joined immediately prior to the vortex split by a narrow "bridge" with high PV but low windspeeds. The increase in the variability of the windspeeds immediately before the split reflects the existence of low windspeeds along the bridge but high windspeeds elsewhere along the vortex edges; edge windspeeds increase, and their standard deviations decrease, once the bridge is broken and the offspring become separated. As seen above, the offspring at 490 K were short-lived (about 5 and 7 days for the ~~green and blue~~ blue offspring-s and green offspring-p vortices, respectively), ~~during which the windspeeds decreased rapidly~~ with windspeeds along their edges decreasing rapidly. In fact, as seen in Figure 12, a coherent mass of air from the ~~blue~~ green offspring-p vortex persisted into April – represented in Figure 14 by the individual purple points labeled "transient", which mark the days on which the area of this region was larger than the 84°EqL cutoff (these can be seen as regions labeled 4, 5, 6, 7, and 8 at 490 K in the supplemental animation). The windspeeds around the edge of the parent vortex (black) remained stronger, though generally decreasing, into late April. A somewhat similar picture is seen at 550 K, with the windspeeds around the single ~~offspring~~ offspring-p vortex (green) being weaker than those bounding the parent vortex, and the parent outliving the offspring; however, the ~~offspring~~ offspring-p vortex at this level was much longer lived than those at 490 K. The evolution of vortex edge windspeeds is thus consistent with that of the transport barriers seen ~~in the mixing diagnostics (~~above in sPV gradients, K_{eff}, and M~~) shown above~~.

The evolution of trace gases in the individual vortices is also consistent with the picture of mixing and vortex breakup seen above. At 490 K, N_2O values were substantially higher in the blue offspring vortex, which persisted slightly longer than the green one, but was still rapidly sheared out into an elongated shape and weakened (as indicated by decreasing windspeeds). Examination of reverse domain filling (RDF, Sutton et al., 1994) maps initialized with MLS data (not shown) suggests that the rapid N_2O increase in the blue vortex in the last two days may be an artifact of MLS not sampling the low values in the narrowest part of the vortex as it was sheared out. Figure 12 (e.g., row A, columns 3 and 4) shows rapid and widespread dispersal of the air from both blue and green offspring vortices, but with some of the air from the blue vortex remaining relatively coherent in a small region even after that vortex was no longer defined. H_2O values were higher in the green offspring vortex because the air in that vortex came from nearer the edge of the parent vortex, rather than from the core where H_2O was strongly depleted (Figure 12, row A, column 1). Average H_2O in the blue offspring vortex was close to that in the parent (black) vortex, consistent with that air coming from somewhat deeper in the parent vortex; this is also consistent with the appearance in Figure 6 of a "path" of low water crossing the vortex edge at the time of the split. Ozone was higher in both the green and blue offspring than in the parent because the air originated in the high O_3 collar near the vortex edge. It was highest in the green vortex because that air came from farther out towards the region of the O_3 maximum (see Figure 6). As was the case for N_2O, the increase in the blue vortex in the last few days may be exaggerated by MLS sampling "missing" a narrow filament of vortex air.

At 550 K, N_2O values were consistently higher in the single (green) offspring vortex than in the parent, indicating more extravortex or vortex edge air than in the parent, as shown in Figure 13 (row A, column 1). That air, however, remained largely confined within that vortex after the split (Figure 13, row A, columns 3 and 4), consistent with relatively constant N_2O mixing

ratios, and suggesting little additional mixing. RDF maps (not shown) at this level do not show obvious evidence of MLS measurements missing filaments of vortex air. There was much less dehydration than at 490 K (see, e.g., Figure 4), so vortex values carried into the green offspring vortex were substantially higher than extravortex values, and the anticorrelation seen between N_2O and H_2O in that offspring vortex is consistent with this morphology. Low ozone values extended out to the vortex edge at 550 K (e.g., Figure 7), and thus the offspring carried very low ozone values with it. This offspring vortex was long-lived, and, though it shrank to an area too small to be cataloged a few days sooner than the parent, the air within both it and the parent remained coherent into late April (~~Figure 13, row C, columns 3 and 4~~not shown). Higher ozone air was drawn up around the parent vortex later on (e.g., Figures 11, and 13, row B, columns 3 and 4), consistent with the offspring vortex retaining lower ozone.

Examination of similar vortex averages of the shorter-lived species HNO_3, HCl, ~~ClO, and HNO(not shown),~~ and ClO indicates that the values of those species remained very nearly the same ~~in~~ across all offspring vortices, and thus their evolution in each offspring vortex closely resembles that shown in Figures 2b, d, and e. Furthermore, RDF maps indicate that the range of values in the small offspring vortices remained very close to those in the initialization fields 12 days earlier (not shown). This provides further evidence that the air in the offspring vortices was confined by an effective transport barrier as long ~~at~~ as those vortices remained ~~coherent~~intact. Thus, except in the period immediately surrounding the split, rapidly decreasing ClO and increasing HCl in all offspring resulted primarily from photochemical deactivation. ~~While~~ Small non-zero ~~, albeit small,~~ values of ClO are apparent in the vortex averages through March (e.g., Figure 2~~) are apparent in the vortex averages through March, the area~~ e), but the area of those vortices in which additional chemical loss could occur was small, less than 4% and 2% of the hemisphere at 490 K and 550 K, respectively.

5 Summary and Conclusions

We have analyzed meteorological fields from the MERRA-2 reanalysis and trace gas data from the Aura Microwave Limb Sounder (MLS) to provide an overview of the exceptionally cold 2015/16 winter and a detailed description of the ~~the~~ vortex breakup in a major final SSW ("major final warming" or MFW) that prevented chemical ozone loss from reaching record high values. Our analyses utilized several mixing diagnostics, as well as a new package (CAVE-ART) for characterizing multiple vortex regions.

The 2015/16 Arctic winter was the coldest on record in December through early February. Lower stratospheric temperatures were at or near a record lows from late December into early February, and far below average from December through mid-March. A substantial region of temperatures below the ice PSC threshold was present continuously from late December through early February, far longer than during any previously observed Arctic winter: The winter mean volume of air below the ice PSC threshold was over twice that previously seen. The chemical ozone loss potential, measured by the commonly used metric of volume of air below the chlorine activation threshold, was nearly identical to that in 2010/11 (when unprecedented Arctic ozone loss occurred). The evolution of trace gases from MLS is consistent with the exceptional meteorological conditions: Vortex-wide dehydration was present between about 410 K and 520 K potential temperature, something never before observed

in the Arctic. Denitrification was also exceptional, and extensive chlorine activation and chemical ozone loss began earlier than in all but one previous winter (2012/2013, Figure 2d–f).

That lower stratospheric ozone loss did not reach ~~values comparable to those~~ the extent of that in spring 2011 was primarily due to the occurrence of an MFW beginning in early March 2016. This event had two critical consequences: First, while the ~~the~~ total volume of cold air during the winter was similar to that in 2010/11, that cold period ended significantly earlier in the winter in 2016, when ozone loss was slower due to less sunlight exposure. Second, the sudden vortex breakup in the MFW resulted in rapid dispersal of chemically processed air from the vortex and consequently curtailed chemical processing, which might have lingered for some time if chlorine had remained confined in a relatively large intact vortex and thus deactivated more gradually.

The Arctic winter meteorology in 2015/16 was so ~~remarkable~~ anomalous that extensive study of numerous processes will be needed to fully characterize its consequences. In this paper we focus on one aspect of this exceptional winter: a detailed description of the event that limited ozone loss to an amount that, while larger than typical in the Arctic, was not unprecedented – the MFW and vortex breakup in early March. The MFW itself was ~~an unusual SSW~~remarkable: The major SSW criteria were fulfilled when the vortex was a single elongated entity displaced far off the pole ~~(a typical "displacement" SSW as defined by Charlton and Pol~~ ~~but~~ in the middle stratosphere (typical of a "displacement" SSW as defined by Charlton and Polvani, 2007) . However, the displacement and distortion at that time were much less pronounced in the lower stratosphere and a few days later the vortex split over a wide range of altitudes covering most of the stratosphere~~(behavior typical of a "split" SSW, e.g., Matthewman et al., 2009) . Moreover,~~ ; in a narrow range of levels in the lower stratosphere ~~near~~ from ∼450 ~~K~~ to 550 K ~~,~~ that split was into three pieces. Early and abrupt final warmings are relatively uncommon, with 13 others before 1 April, and only five of those before mid-March, reported since 1958 (Hu et al., 2014) . The only other MFW during the Aura mission began around 10–12 March 2005, and halted ozone loss in the unusually cold 2004/2005 winter (see, e.g., Manney et al., 2006a, b; Hu et al., 2014) ; the morphology of the vortex breakup in 2005 showed similarities to that in 2016, in that the vortex was first strongly displaced in the middle stratosphere and then split, albeit into only two pieces, over a deep altitude region. In 2005, however, there had been no extensive denitrification or dehydration, and chlorine deactivation had begun concurrently with increasing temperatures about three weeks before the MFW (Singleton et al., 2007; Santee et al., 2008) .

In the middle stratosphere (exemplified herein by 850 K), transport and mixing diagnostics and MLS trace gases show that by the time of the MFW the vortex had already shrunk, and a strong Aleutian anticyclone and vigorous surf zone formed, consistent with climatology. In mid-March, about a week after the MFW began, the vortex split into two very unequal pieces; the larger ~~one~~ parent vortex rapidly sheared out and dispersed, while a ~~very~~ small coherent remnant of the ~~other remained intact with relatively little mixing into early April~~offspring lingered through late March. The evolution of MLS CO and H_2O in the decaying vortices indicates that air within them remained well confined as long as they were intact. Snapshots of the function M show a picture consistent with the ~~the~~ trace gas evolution, in that the vortex transport barrier decayed rapidly after the MFW onset.

The breakup of and dispersal of air from the vortex in the lower stratosphere was slower and more episodic, with largest changes in the short period surrounding the vortex split. Some of the specific consequences of the lower stratospheric vortex

evolution (shown here at 490 and 550 K) during the MFW for transport, mixing, and dispersal of chemically processed air are as follows:

- At 490 K, two small offspring split off the main vortex in mid-March, but persisted for only about a week.
- At 550 K, the vortex split into two pieces, both of which remained well defined for over a month after the split.
- Mixing increased only slightly after the onset of the MFW around 7 March, but extensive mixing occurred in the few days during and after the vortex split in mid-March.
- Immediately following the split the total vortex area decreased by 30% to 40%, with the largest offspring covering about 4% of the hemisphere, and smaller offspring an additional 1 to 2% of the hemisphere.
- Following this period of intensive vortex erosion and mixing, air remained well-confined within the remaining offspring vortices.
- Abundances of MLS N_2O and O_3 in the offspring vortices at 550 K remained closer to those in the parent vortex than at 490 K, indicating less mixing; this is consistent with the stronger transport barrier after the vortex split seen ~~in the mixing diagnostics~~ at that level, and with the greater persistence of the offspring vortices.
- ClO rapidly decayed in the offspring vortices as a result of a combination of rapid deactivation and dispersal of vortex air during the split.
- The evolution of ozone in the offspring vortices was dependent on the region within the parent vortex where the air originated, such that the offspring at 490 K contained higher values characteristic of the collar of undepleted ozone along the vortex edge, whereas at 550 K, low ozone values extended farther out into the vortex edge region and the smaller, but stronger, offspring vortex carried lower ozone than the parent.
- The "function M," when binned as a function of EqL, evolved consistently with the bulk transport barrier/mixing diagnostics (sPV gradients and effective diffusivity), but also revealed local variations (including relative strength of the offspring vortices, variations in the transport barrier around the vortex edge, and the dissolution of the individual vortices) that are consistent with the synoptic evolution of MLS trace gases.

In both the lower and middle stratosphere the mixing following the MFW was primarily via erosion and filamentation of the vortices as long as they remained intact. This resulted in wide dispersal and rapid mixing of air formerly in the vortex, but ~~little~~ in general, transport of extra-vortex air ~~intruding~~ into the vortex regions ~~while they remained well-defined~~was rare.

The major final SSW in early March 2016 was a remarkable finale to an already exceptional Arctic winter. The results presented here suggest the need for many further studies to assess not only how well the evolution of the vortex and trace gases throughout the 2015/16 winter fits with our current understanding of and ability to model lower stratospheric polar chemical processes, but also provides a unique addition to the already wide variety of natural experiments conducted

via the immense variability in Arctic polar vortex evolution, longevity, and breakup. This new information is important for improving our detailed understanding of variations in dispersal of ozone depleted and/or chemically activated air from the vortex and its implications for present and future global ozone distributions. Further studies will include detailed analyses using similar methods to this work comparing the vortex breakup in 2016 with that in other winters, both Arctic and Antarctic. This is particularly interesting given reported differences between years with early and late Arctic final warmings ~~, which~~ (e.g. Waugh and Rong, 2002; Akiyoshi and Zhou, 2007) . While these have not, in general, ~~accounted for the suddenness of those final warmings(e.g. Waugh and Rong, 2002; Akiyoshi and Zhou, 2007) ; the 2011 vortex breakup, for example, was very~~ considered the abruptness of the final warmings, more recent studies indicate substantial circulation differences following sudden and gradual final warmings: Frozen-in anticyclones formed following the mid-March 2005 MFW and the late, but ~~also quite sudden, whereas late final warmings in 2007 and 2008 were more gradual~~sudden, 2011 vortex breakup (e.g., Manney et al., 2006a; Allen et al., 2012; Thiéblemont et al., 2013) , and observational and modeling studies indicate than an abrupt final warming is one of the conditions necessary for a frozen-in anticyclone to occur (Thiéblemont et al., 2013, 2016) . In contrast to the Arctic, chlorine is typically deactivated well before the Antarctic vortex breakup (e.g., Manney et al., 2005; Santee et al., 2008), but the details and timing of that breakup still have important consequences – not only for local ozone minima over populated areas, but also for dilution of midlatitude ozone (e.g., Ajtić et al., 2004) and for radiative impacts of the Antarctic ozone hole (e.g., Polvani et al., 2011; WMO, 2014). Additional Lagrangian transport and air mass history studies, combined with analyses of Aura data over ~~it's~~ its (so far) dozen year mission, will help quantify the fate of activated and ozone depleted air as the polar vortices decay.

In light of the 2012/13 winter, when an exceptionally strong vortex-split SSW resulted in record early winter ozone loss, and the 2014/15 winter, when a very brief, minor SSW resulted in record high vortex ozone values, the importance of the early and abrupt major final SSW in limiting ozone loss in spring 2016 once again emphasizes the complexity of the interactions between these extreme dynamical events and chemical processes in the stratospheric polar vortex. In each of these winters, the SSW events had dramatic consequences that were largely unanticipated. SSW characteristics are also expected to evolve with the changing climate (e.g., Charlton-Perez et al., 2008; McLandress and Shepherd, 2009). We should thus expect the Arctic wintertime meteorology, and its impact on chemical processing, to continue to surprise us in the future, making continued comprehensive monitoring of stratospheric composition a critical priority.

Acknowledgements. We thank members of the MLS team at JPL for data processing/analysis, data management, and computational support (especially Luis Millan, Ryan Fuller, and Brian Knosp), for producing/providing the MLS dataset, and for helpful discussions (especially Nathaniel Livesey, Michelle Santee, and Michael Schwartz). We also thank Ken Minschwaner for helpful discussions and comments on the manuscript. MERRA-2 reanalysis data were provided by NASA's GMAO, led by Steven Pawson, and we especially thank Kris Wargan for his helpful comments and assistance with usage of those. Andreas Dörnbrack, Rémi Thiémblemont, and an anonymous referee provided comments that were very helpful in improving the paper. GLM's work on this paper was funded by and conducted under a contract from the Aura MLS Project at the Jet Propulsion Laboratory. Both authors contributed equally to this paper.

The datasets used are publicly available, the MLS data from http://disc.sci.gsfc.nasa.gov/Aura/data-holdings/MLS/index.shtml, corresponding DMP files from http://mls.jpl.nasa.gov, and the GMAO reanalysis data from http://disc.sci.gsfc.nasa.gov/daac-bin/DataHoldings.pl.

References

Ajtić, J., Connor, B. J., Lawrence, B. N., Bodeker, G. E., Hoppel, K. W., Rosenfield, J. E., and Heuff, D. N.: Dilution of the Antarctic ozone hole into southern midlatitudes, 1998-2000, J. Geophys. Res., 109, D17107, doi:10.1029/2003JD004500, 2004.

Akiyoshi, H. and Zhou, L. B.: Midlatitude and high-latitude N_2O distributions in the Northern Hemisphere in early and late Arctic polar vortex breakup years, J. Geophys. Res., 112, D18305, doi:10.1029/2007JD008491, 2007.

Allen, D. R. and Nakamura, N.: A seasonal climatology of effective diffusivity in the stratosphere, J. Geophys. Res., 106, 7917–7935, 2001.

Allen, D. R. and Nakamura, N.: Dynamical reconstruction of the record low column ozone over Europe on 30 November 1999, Geophys. Res. Lett., 29, 1362, doi:10.1029/2002GL014935, 2002.

Allen, D. R. and Nakamura, N.: Tracer Equivalent Latitude: A Diagnostic tool for isentropic transport studies, J. Atmos. Sci., 60, 287–304, 2003.

Allen, D. R., Douglass, A. R., Nedoluha, G. E., and Coy, L.: Tracer transport during the Arctic stratospheric final warming based on a 33-year (1979-2011) tracer equivalent latitude simulation, Geophys. Res. Lett., 39, L12801, doi:10.1029/2012GL051930, 2012.

Andrews, D. G.: Some comparisons between the middle atmosphere dynamics for the southern and northern hemispheres, Pure and Appl. Geophys., 130, 213–232, 1989.

Andrews, D. G., Holton, J. R., and Leovy, C. B.: Middle Atmosphere Dynamics, Academic Press, San Diego, Calif., 1st edn., 1987.

Arnone, E., Castelli, E., Papandrea, E., Carlotti, M., and Dinelli, B. M.: Extreme ozone depletion in the 2010–2011 Arctic winter stratosphere as observed by MIPAS/ENVISAT using a 2-D tomographic approach, Atmos. Chem. Phys., 12, 9149–9165, 2012.

Balibrea-Iniesta, F., Curbelo, J., García-Garrido, V. J., Lopesino, C., Mancho, A. M., Mendoza, C., and Wiggins, S.: Response to: "Limitations of the Method of Lagrangian Descriptors" [arXiv:1510.04838], ArXiv e-prints, http://arxiv.org/abs/1602.04243, 2016.

Black, R. X. and McDaniel, B. A.: The Dynamics of Northern Hemisphere Stratospheric Final Warming Events, Journal of the Atmospheric Sciences, 64, 2932–2946, 2007.

Bloom, S. C., Takacs, L. L., da Silva, A. M., and Ledvina, D.: Data assimilation using incremental analysis updates, Mon. Weather Rev., 124, 1256–1271, 1996.

Blume, C., Matthes, K., and Horenko, I.: Supervised Learning Approaches to Classify Sudden Stratospheric Warming Events, J. Atmos. Sci., 69, 1824–1840, 2012.

Bosilovich, M., Akella, S., Coy, L., Cullather, R., Draper, C., Gelaro, R., Kovach, R., Liu, Q., Molod, A., Norris, P., Wargan, K., Chao, W., Reichle, R., Takacs, L., Vikhliaev, Y., Bloom, S., Collow, A., Firth, S., Labow, G., Partyka, G., Pawson, S., Reale, O., Schubert, S. D., and Suarez, M.: MERRA-2: Initial Evaluation of the Climate, Series on Global Modeling and Data Assimilation, NASA/TM–2015-104606, Vol. 43, NASA, 2015.

Butchart, N. and Remsberg, E. E.: The area of the stratospheric polar vortex as a diagnostic for tracer transport on an isentropic surface, J. Atmos. Sci., 43, 1319–1339, 1986.

Butler, A. H., Seidel, D. J., Hardiman, S. C., Butchart, N., Birner, T., and Match, A.: Defining Sudden Stratospheric Warmings, Bull. Am. Meteor. Soc., 96, 1913–1928, doi:10.1175/BAMS-D-13-00173.1, 2015.

Charlton, A. J. and Polvani, L. M.: A New Look at Stratospheric Sudden Warmings. Part I: Climatology and Modeling Benchmarks, J. Clim., 20, 449–469, 2007.

Charlton-Perez, A. J., Polvani, L. M., Austin, J., and Li, F.: The frequency and dynamics of stratospheric sudden warmings in the 21st century, J. Geophys. Res., 113, D16116, doi:10.1029/2007JD009571, 2008.

Chen, P., Holton, J. R., O'Neill, A., and Swinbank, R.: Quasi-horizontal transport and mixing in the Antarctic stratosphere, J. Geophys. Res., 99, 16,851–16,866, 1994.

Davies, S., Chipperfield, M. P., Carslaw, K. S., Sinnhuber, B.-M., Anderson, J. G., Stimpfle, R. M., Wilmouth, D. M., Fahey, D. W., Popp, P. J., Richard, E. C., von der Gathen, P., Jost, H., and Webster, C. R.: Modeling the effect of denitrification on Arctic ozone depletion during winter 1999/2000, J. Geophys. Res., 107, SOL–65–1Fe–SOL–65–18, 2002.

de la Cámara, A., Mancho, A. M., Ide, K., Serrano, E., and Mechoso, C. R.: Routes of Transport across the Antarctic Polar Vortex in the Southern Spring, J. Atmos. Sci., 69, 741–752, doi:10.1175/JAS-D-11-0142.1, http://dx.doi.org/10.1175/JAS-D-11-0142.1, 2012.

de la Cámara, A., Mechoso, C. R., Mancho, A. M., Serrano, E., and Ide, K.: Isentropic Transport within the Antarctic Polar-Night Vortex: Rossby Wave Breaking Evidence and Lagrangian Structures, J. Atmos. Sci., 70, 2982–3001, doi:10.1175/JAS-D-12-0274.1, http://dx.doi.org/10.1175/JAS-D-12-0274.1, 2013.

Dörnbrack, A., Pitts, M. C., Poole, L. R., Orsolini, Y. J., Nishii, K., and Nakamura, H.: The 2009–2010 Arctic stratospheric winter — general evolution, mountain waves and predictability of an operational weather forecast model, Atmos. Chem. Phys., 12, 3659–3675, 2012.

Douglass, A. R., Schoeberl, M. R., Stolarski, R. S., Waters, J. W., III, J. M. R., Roche, A. E., and Massie, S. T.: Interhemispheric differences in springtime production of HCl and $ClONO_2$ in the polar vortices, J. Geophys. Res., 100, 13,967–13,978, 1995.

Dunkerton, T. J. and Delisi, D. P.: Evolution of potential vorticity in the winter stratosphere of January-February 1979, J. Geophys. Res., 91, 1199–1208, 1986.

García-Garrido, V., Ramos, A., Mancho, A., Coca, J., and Wiggins, S.: A dynamical systems perspective for a real-time response to a marine oil spill, Marine Pollution Bulletin, 112, 201 – 210, doi:http://dx.doi.org/10.1016/j.marpolbul.2016.08.018, http://www.sciencedirect.com/science/article/pii/S0025326X16306506, 2016.

Global Modeling and Assimilation Office (GMAO): MERRA-2 inst3_3d_asm_Nv: 3d, 3-Hourly,Instantaneous, Model-Level, Assimilation, Assimilated Meteorological Fields V5.12.4, version 5.12.4, Greenbelt, MD, USA, Goddard Earth Sciences Data and Information Services Center (GES DISC), Accessed 1 November 2015, doi:10.5067/WWQSXQ8IVFW8, 2015.

Guha, A., Mechoso, C. R., Konor, C. S., and Heikes, R. P.: Modeling Rossby Wave Breaking in the Southern Spring Stratosphere, Journal of the Atmospheric Sciences, 73, 393–406, doi:10.1175/JAS-D-15-0088.1, 2016.

Haller, G.: Lagrangian Coherent Structures, Annual Review of Fluid Mechanics, 47, 137–162, doi:10.1146/annurev-fluid-010313-141322, 2015.

Harvey, V. L., Pierce, R. B., Fairlie, T. D., and Hitchman, M. H.: A Climatology of Stratospheric polar vortices and anticyclones, J. Geophys. Res., 107, 4442, doi:1029/2001JD001471, 2002.

Harvey, V. L., Pierce, R. B., Hitchman, M. H., Randall, C. E., and Fairlie, T. D.: On the distribution of ozone in stratospheric anticyclones, J. Geophys. Res., 109, D24308, doi:10.1029/2004JD004992, 2004.

Haynes, P. and Shuckburgh, E.: Effective diffusivity as a diagnostic of atmospheric transport 1. Stratosphere, J. Geophys. Res., 105, 22,777–22,794, 2000.

Hintsa, E. J. et al.: Dehydration and denitrification in the Arctic polar vortex during the 1995-1996 winter, Geophys. Res. Lett., 25, 501–504, 1998.

Hoffmann, P., Singer, W., and Keuer, D.: Variability of the mesospheric wind fields at middle and Arctic latitudes in winter and its relation to stratospheric circulation disturbances, J. Atmos. Sol.-Ter. Phys., 64, 1229–1240, 2002.

Hu, J., Ren, R., and Xu, H.: Occurrence of Winter Stratospheric Sudden Warming Events and the Seasonal Timing of Spring Stratospheric Final Warming, J. Atmos. Sci., 71, 2319–2334, 2014.

Konopka, P., Grooß, J.-U., Baush, S., Müller, R., McKenna, D. S., Morgenstern, O., and Orsolini, Y.: Dynamics and chemistry of vortex remnants in late Arctic spring 1997 and 2000: Simulations with the Chemical Lagrangian Model of the Stratosphere (CLaMS), Atmos. Chem. Phys., 3, 839–849, 2003.

Labitzke, K.: On the Interannual variability of the middle stratosphere during the Northern winters, J. Met. Soc. Japan, 60, 124–139, 1982.

Labitzke, K.: The solar signal of the 11-year sunspot cycle in the stratosphere differences between the northern and southern summers, J. Meteor. Soc. Japan, 80, 963–971, 2002.

Lawrence, Z. D. and Manney, G. L.: Characterization and Analyses of Multiple Vortices: The CAVE-ART package, *In preparation*, 2016.

Lawrence, Z. D., Manney, G. L., Minschwaner, K., Santee, M. L., and Lambert, A.: Comparisons of polar processing diagnostics from 34 years of the ERA-Interim and MERRA reanalyses, Atmos. Chem. Phys., 15, 3873–3892, 2015.

Leovy, C. B., Sun, C., Hitchman, M. H., Remsberg, E. E., III, J. M. R., Gordley, L. L., Gille, J. C., and Lyjak, L. V.: Transport of ozone in the middle stratosphere: Evidence for planetary wave breaking, J. Atmos. Sci., 42, 230–244, 1985.

Livesey, N. J., Read, W. G., Wagner, P. A., Froidevaux, L., Lambert, A., Manney, G. L., Millán Valle, L. F., Pumphrey, H. C., Santee, M. L., Schwartz, M. J., Wang, S., Fuller, R. A., Jarnot, R. F., Knosp, B. W., and Martinez, E.: EOS MLS Version 4.2x Level 2 data quality and description document, Tech. rep., JPL, available from http://mls.jpl.nasa.gov/, 2015a.

Livesey, N. J., Santee, M. L., and Manney, G. L.: A Match-based approach to the estimation of polar stratospheric ozone loss using Aura Microwave Limb Sounder observations,, Atmos. Chem. Phys., 15, 9945–9963, 2015b.

Lowe, D. and MacKenzie, A. R.: Polar stratospheric cloud microphysics and chemistry, Journal of Atmospheric and Solar-Terrestrial Physics, 70, 13 – 40, doi:http://dx.doi.org/10.1016/j.jastp.2007.09.011, http://www.sciencedirect.com/science/article/pii/S1364682607002520, 2008.

Madrid, J. A. J. and Mancho, A. M.: Distinguished trajectories in time dependent vector fields, Chaos, 19, 013111, doi:http://dx.doi.org/10.1063/1.3056050, http://scitation.aip.org/content/aip/journal/chaos/19/1/10.1063/1.3056050, 2009.

Mancho, A. M., Wiggins, S., Curbelo, J., and Mendoza, C.: Lagrangian descriptors: A method for revealing phase space structures of general time dependent dynamical systems, Communications in Nonlinear Science and Numerical Simulation, 18, 3530 – 3557, doi:http://dx.doi.org/10.1016/j.cnsns.2013.05.002, http://www.sciencedirect.com/science/article/pii/S1007570413002037, 2013.

Manney, G. L., Zurek, R. W., O'Neill, A., and Swinbank, R.: On the motion of air through the stratospheric polar vortex, J. Atmos. Sci., 51, 2973–2994, 1994.

Manney, G. L., Froidevaux, L., Waters, J. W., , Gille, J. C., Zurek, R. W., Kumer, J. B., Mergenthaler, J. L., Roche, A. E., O'Neill, A., and Swinbank, R.: Formation of low-ozone pockets in the middle stratospheric anticyclone during winter, J. Geophys. Res., 100, 13,939–13,950, 1995.

Manney, G. L., Michelsen, H. A., Santee, M. L., Gunson, M. R., Irion, F. W., Roche, A. E., and Livesey, N. J.: Polar vortex dynamics during spring and fall diagnosed using trace gas observations from the Atmospheric Trace Molecule Spectroscopy instrument, J. Geophys. Res., 104, 18,841–18,866, 1999.

Manney, G. L., Santee, M. L., Livesey, N. J., Froidevaux, L., Read, W. G., Pumphrey, H. C., Waters, J. W., and Pawson, S.: EOS Microwave Limb Sounder observations of the Antarctic polar vortex breakup in 2004, Geophys. Res. Lett., 32, L12811, doi:10.1029/2005GL022823, 2005.

Manney, G. L., Livesey, N. J., Jimenez, C. J., Pumphrey, H. C., Santee, M. L., MacKenzie, I. A., Froidevaux, L., and Waters, J. W.: EOS MLS observations of "frozen-in" anticyclonic air in Arctic summer, Geophys. Res. Lett., 33, L06810, doi:10.1029/2005GL025418, 2006a.

Manney, G. L., Santee, M. L., Froidevaux, L., Hoppel, K., Livesey, N. J., and Waters, J. W.: EOS MLS observations of ozone loss in the 2004-2005 Arctic winter, Geophys. Res. Lett., 33, L04802, doi:10.1029/2005GL024494, 2006b.

Manney, G. L., Daffer, W. H., Zawodny, J. M., Bernath, P. F., Hoppel, K. W., Walker, K. A., Knosp, B. W., Boone, C., Remsberg, E. E., Santee, M. L., Harvey, V. L., Pawson, S., Jackson, D. R., Deaver, L., McElroy, C. T., McLinden, C. A., Drummond, J. R., Pumphrey, H. C., Lambert, A., Schwartz, M. J., Froidevaux, L., McLeod, S., Takacs, L. L., Suarez, M. J., Trepte, C. R., Cuddy, D. C., Livesey, N. J., Harwood, R. S., and Waters, J. W.: Solar occultation satellite data and derived meteorological products: Sampling issues and comparisons with Aura Microwave Limb Sounder, J. Geophys. Res., 112, doi:10.1029/2007JD008709, 2007.

Manney, G. L., Santee, M. L., Rex, M., Livesey, N. J., Pitts, M. C., Veefkind, P., Nash, E. R., Wohltmann, I., Lehmann, R., Froidevaux, L., Poole, L. R., Schoeberl, M. R., Haffner, D. P., Davies, J., Dorokhov, V., Gernandt, H., Johnson, B., Kivi, R., Kyrö, E., Larsen, N., Levelt, P. F., Makshtas, A., McElroy, C. T., Nakajima, H., Parrondo, M. C., Tarasick, D. W., von der Gathen, P., Walker, K. A., and Zinoviev, N. S.: Unprecedented Arctic Ozone Loss in 2011, Nature, 478, 469–475, 2011.

Manney, G. L., Lawrence, Z. D., Santee, M. L., Livesey, N. J., Lambert, A., and Pitts, M. C.: Polar processing in a split vortex: Arctic ozone loss in early winter 2012/2013, Atmos. Chem. Phys., 15, 4973–5029, 2015a.

Manney, G. L., Lawrence, Z. D., Santee, M. L., Read, W. G., Livesey, N. J., Lambert, A., Froidevaux, L., Pumphrey, H. C., and Schwartz, M. J.: A minor sudden stratospheric warming with a major impact: Transport and polar processing in the 2014/2015 Arctic winter, Geophys. Res. Lett., 42, 7808–7816, doi:10.1002/2015GL065864, 2015b.

Marchand, M., Lefevre, S. B., Hauchecorne, A., Godin-Beekmann, S., and Chipperfield, M.: Model simulations of the northern extravortex ozone column: Influence of past changes in chemical composition, J. Geophys. Res., 109, D02310, doi:10.1029/2003JD003634, 2004.

Matthewman, N. J., Esler, J. G., Charlton-Perez, A. J., and Polvani, L. M.: A New look at stratospheric sudden warmings. Part III: Polar vortex evolution and vertical structure, J. Clim., 22, 1566–1585, 2009.

McIntyre, M. E. and Palmer, T. N.: The “surf zone" in the stratosphere, J. Atmos. and Terr. Phys., 46, 825–849, 1984.

McLandress, C. and Shepherd, T. G.: Impact of Climate Change on Stratospheric Sudden Warmings as Simulated by the Canadian Middle Atmosphere Model, J. Clim., 22, 5449–5463, 2009.

Mendoza, C. and Mancho, A. M.: Hidden Geometry of Ocean Flows, Phys. Rev. Lett., 105, doi:10.1103/PhysRevLett.105.038501, http://link.aps.org/doi/10.1103/PhysRevLett.105.038501, 2010.

Mitchell, D. M., Charlton-Perez, A. J., and Gray, L. J.: Characterizing the Variability and Extremes of the stratospheric polar vortices using 2D moment analysis, J. Atmos. Sci., 68, 1194–1213, 2011.

Molod, A., Takacs, L., Suarez, M., and Bacmeister, J.: Development of the GEOS-5 Atmospheric General Circulation Model: Evolution from MERRA to MERRA2, Geosci. Model Dev., 8, 1339–1356, 2015.

Nakamura, N.: Two-dimensional mixing, edge formation, and permeability diagnosed in area coordinates, J. Atmos. Sci., 53, 1524–1537, 1996.

Naujokat, B., Krüger, K., Matthes, K., Hoffmann, J., Kunze, M., and Labitzke, K.: The early major warming in December 2001 – exceptional?, Geophys. Res. Lett., 29, 2023, doi:10.1029/2002GL015316, 2002.

Polvani, L. M., Waugh, D. W., Correa, G. J., and Son, S.-W.: Stratospheric ozone depletion: The main driver of twentieth-century atmospheric circulation changes in the Southern Hemisphere, J. Clim., 24, 795–812, 2011.

Prather, M. and Jaffe, A. H.: Global impact of the Antarctic ozone hole: Chemical propagation, J. Geophys. Res., 95, 3473–3492, 1990.

Rex, M., Salawitch, R. J., Gathen, P., Harris, N. R., Chipperfield, M. P., and Naujokat, B.: Arctic ozone loss and climate change, Geophys. Res. Lett., 31, L04116, doi:10.1029/2003GL018844, 2004.

Ruiz-Herrera, A.: Some examples related to the method of Lagrangian descriptors, Chaos, 25, 063112, doi:http://dx.doi.org/10.1063/1.4922182, http://scitation.aip.org/content/aip/journal/chaos/25/6/10.1063/1.4922182, 2015.

Santee, M. L., Froidevaux, L., Manney, G. L., Read, W. G., Waters, J. W., Chipperfield, M. P., Roche, A. E., Kumer, J. B., Mergenthaler, J. L., and III, J. M. R.: Chlorine deactivation in the lower stratospheric polar regions during late winter: Results from UARS, J. Geophys. Res., 101, 18,835–18,859, 1996.

Santee, M. L., Tabazadeh, A., Manney, G. L., Salawitch, R. J., Froidevaux, L., Read, W. G., and Waters, J. W.: UARS MLS HNO_3 observations: Implications for Antarctic polar stratospheric clouds, J. Geophys. Res., 103, 13,285–13,314, 1998.

Santee, M. L., MacKenzie, I. A., Manney, G. L., Chipperfield, M. P., Bernath, P. F., Walker, K. A., Boone, C. D., Froidevaux, L., Livesey, N. J., and Waters, J. W.: A study of stratospheric chlorine partitioning based on new satellite measurements and modeling, J. Geophys. Res., 113, D12307, doi:10.1029/2007JD009057, 2008.

Singleton, C. S. et al.: Quantifying Arctic ozone loss during the 2004-2005 winter using satellite observations and a chemical transport model, J. Geophys. Res., 112, D07304, doi:10.1029/2006JD007463, 2007.

Sinnhuber, B.-M., Stiller, G., Ruhnke, R., von Clarmann, T., Kellmann, S., and Aschmann, J.: Arctic winter 2010/2011 at the brink of an ozone hole, Geophys. Res. Lett., L24814, doi:10.1029/2011GL049784, 2011.

Smith, M. and McDonald, A. J.: A quantitative measure of polar vortex strength using the function M, J. Geophys. Res., 119, 5966–5985, doi:10.1002/2013JD020572, 2014.

Sutton, R. T., MacLean, H., Swinbank, R., O'Neill, A., and Taylor, F. W.: High-resolution stratospheric tracer fields estimated from satellite observations using Lagrangian trajectory calculations, J. Atmos. Sci., 51, 2995–3005, 1994.

Takacs, L. L., Suárez, M. J., and Todling, R.: Maintaining atmospheric mass and water balance in reanalyses, Q. J. R. Meteorol. Soc., 142, 1565–1573, 2016.

Tan, D. G. H., MacKenzie, P. H. H. A. R., and Pyle, J. A.: The effects of fluid-dynamical stirring and mixing on the deactivation of stratospheric chlorine, J. Geophys. Res., 103, 1585–1605, 1998.

Thiéblemont, R., Orsolini, Y. J., Hauchecorne, A., Drouin, M.-A., and Huret, N.: A Climatology of Frozen-In Anticyclones in the Spring Arctic Stratosphere over the Period 1960–2011, J. Geophys. Res., 118, 1299–1311, doi:10.1002/jgrd.50156, 2013.

Thiéblemont, R., Matthes, K., Orsolini, Y. J., Hauchecorne, A., and Huret, N.: Poleward Transport Variability in the Northern Hemisphere during the Final Stratospheric Warming simulated by CESM(WACCM), J. Geophys. Res., 121, doi:10.1002/2016JD025358, 2016.

Tilmes, S., Müller, R., Engel, A., Rex, M., and Russel, J. M.: Chemical ozone loss in the Arctic and Antarctic stratosphere between 1992 and 2005, Geophys. Res. Lett., 33, doi:10.1029/2006GL026925, 2006.

Waibel, A. E., Peter, T., Carslaw, K. S., Oelhaf, H., Wetzel, G., Crutzen, P. J., Poschl, U., Tsias, A., Reimer, E., and Fischer, H.: Arctic ozone loss due to denitrification, Science, 283, 2064–2069, 1999.

Waters, J. W., Froidevaux, L., Harwood, R. S., Pickett, R. F. J. H. M., Read, W. G., Siegel, P. H., Cofield, R. E., Filipiak, M. J., Flower, D. A., Holden, J. R., Lau, G. K., Livesey, N. J., Manney, G. L., Pumphrey, H. C., Santee, M. L., Wu, D. L., Cuddy, D. T., Lay, R. R., Loo, M. S., Perun, V. S., Schwartz, M. J., Stek, P. C., Thurstans, R. P., Boyles, M. A., Chandra, S., Chavez, M. C., Chen, G.-S., Chudasama, B. V., Dodge, R., Fuller, R. A., Girard, M. A., Jiang, J. H., Jiang, Y., Knosp, B. W., LaBelle, R. C., Lam, J. C., Lee, K. A., Miller, D., Oswald, J. E., Patel, N. C., Pukala, D. M., Quintero, O., Scaff, D. M., Snyder, W. V., Tope, M. C., Wagner, P. A., and Walch, M. J.: The Earth Observing System Microwave Limb Sounder (EOS MLS) on the Aura satellite, *IEEE Trans. Geosci. Remote Sens.*, 44, 1075–1092, 2006.

Waugh, D. W. and Randel, W. J.: Climatology of Arctic and Antarctic polar vortices using elliptical diagnostics, J. Atmos. Sci., 56, 1594–1613, 1999.

Waugh, D. W. and Rong, P.: Interannual variability in the decay of lower stratospheric Arctic vortices, J. Meteor. Soc. Japan, 80, 997–1012, 2002.

WMO: Scientific assessment of ozone depletion: 2014, Global Ozone Res. and Monit. Proj. Rep. 55, Geneva, Switzerland, 2014.

Wofsy, S. C., Salawitch, R. J., Yatteau, J. H., McElroy, M. B., Gandrud, B. W., Dye, J. E., and Baumgardner, D.: Condensation of HNO_3 on falling ice particles: Mechanism for denitrification of the polar stratosphere, Geophys. Res. Lett., 17, 449–452, 1990.

Wohltmann, I. et al.: Uncertainties in modelling heterogeneous chemistry and Arctic ozone depletion in the winter 2009/2010, Atmos. Chem. Phys., 13, 3909–3929, 2013.

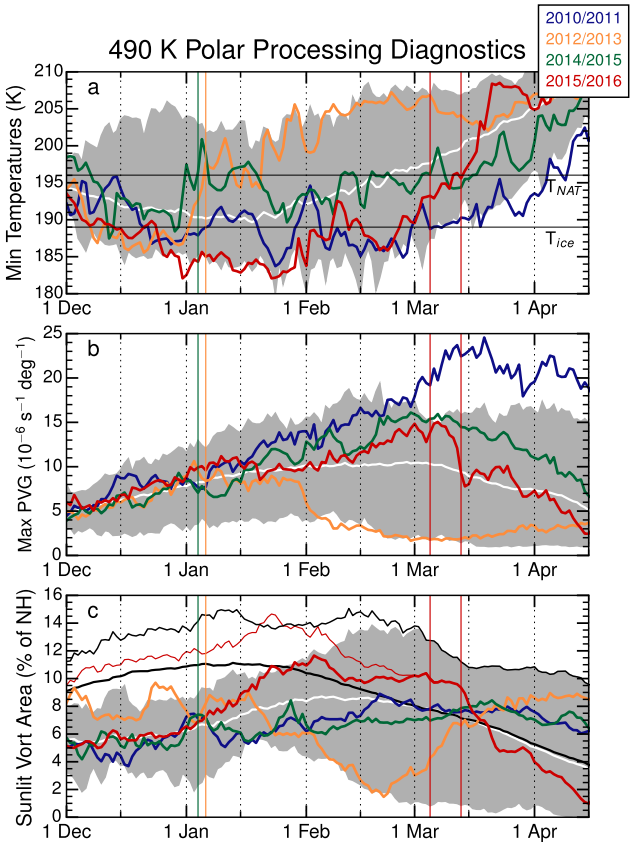

Figure 1. Time series of (a) minimum temperatures, (b) ~~V_{NAT}/V_{Vort}, (c)~~ maximum gradients of scaled potential vorticity as a function of EqL (Max PVG), and (~~d~~c) sunlit area of the polar vortex from MERRA-2 in the 2010/11 (blue), 2012/13 (orange), 2014/15 (green) and 2015/16 (red) Arctic winters compared with the mean (white) and range (grey shading) of other years on record beginning with 1979/80. Thin vertical lines indicate significant SSW dates: 6 January 2013 and 5 March 2016 (first red line) are the dates when major SSW criteria were met in those winters; 4 January is the date when the 2015 minor SSW briefly split the vortex; 13 March (second red line) is the approximate date of the 2016 vortex split. In (a), the thin black horizontal lines indicate the approximate NAT and ice PSC thresholds. In (~~d~~c), in addition to the thick colored lines indicating sunlit vortex area, the thin ~~colored lines indicate~~ red line indicates the total vortex area in 2015/16, with the thick/thin black ~~line~~ lines showing the daily climatological average~~total~~ /maxima of vortex area; at times when the thick and thin red lines coincide, the vortex is fully in sunlight. ~~(a), (c), and (d)~~ All of these diagnostics are ~~from data at~~ shown on the 490 K ~~potential temperature level; (b) includes data integrated from levels between 390 and 580K~~isentropic surface.

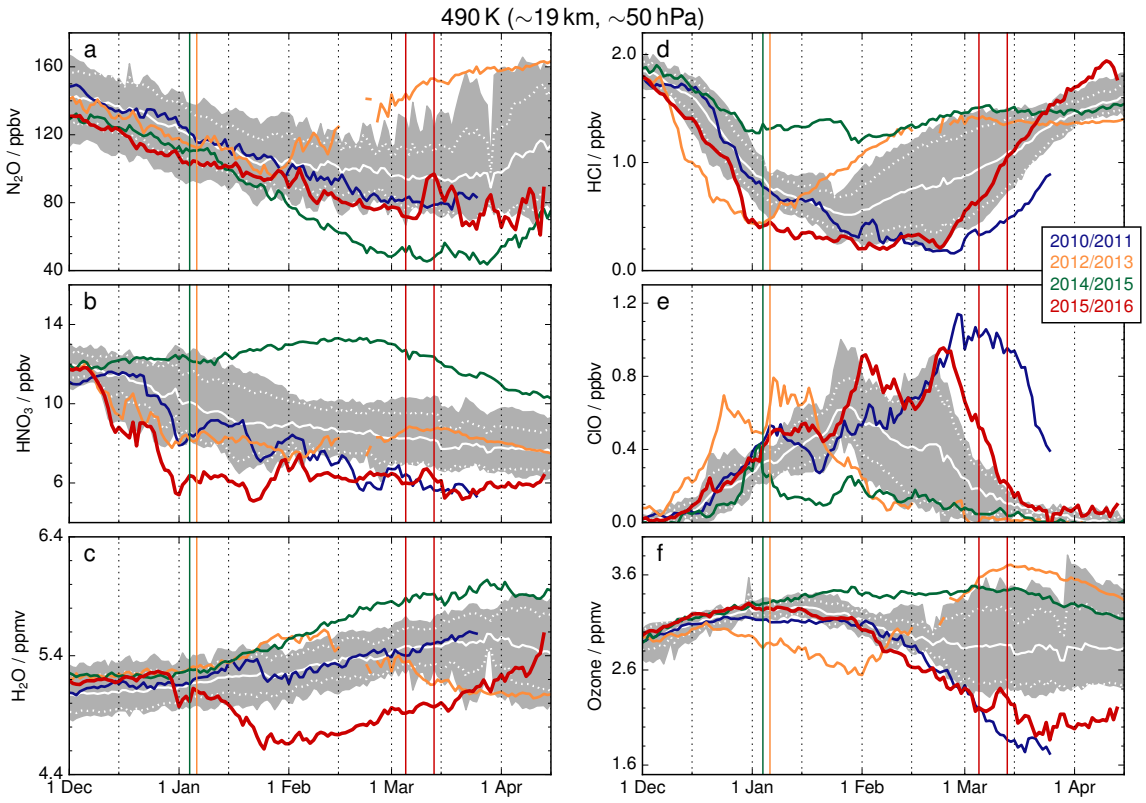

Figure 2. Time series of 490 K MLS vortex averaged N_2O (a), HNO_3 (b), H_2O (c), HCl (d), ClO (e), and ozone (f) in the 2010/11 (blue), 2012/13 (orange), 2014/15 (green) and 2015/16 (red) Arctic winters compared with the mean (solid white), one standard deviation range (dotted white) and minimum/maximum range (grey shading) of other years in the Aura record (beginning with 2004/05). Vertical colored lines are as in Figure 1. These vortex averages are calculated using the sum of the vortex regions identified by CAVE-ART with an 82° EqL cutoff to exclude un-climatological features due to very small vortex regions with anomalous characteristics in some years (the gap in the 2013 line shows a period when the lower stratospheric vortex was undefined by this criterion).

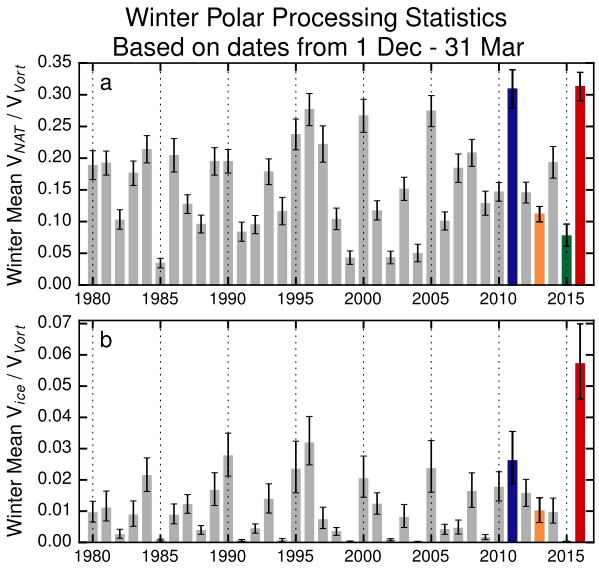

Figure 3. Winter polar processing statistics based on temperatures from the MERRA-2 reanalysis: (a) winter mean V_{NAT}/V_{Vort}, and (b) ~~number of days below T_{NAT} summed over isentropic levels from 390 to 550K, (c)~~ winter mean V_{ice}/V_{Vort}, ~~and (d) number of days below T_{ice} summed over the same levels as (b)~~. All bars are calculated from time series data limited to 1 Dec ~~to~~ through 31 Mar, using isentropic levels between 390 and 580 K (nominally between ~380 K and 565 K, using midpoint levels to estimate altitudes). ~~All year~~ Error bars represent the sensitivity of these diagnostics to using $\pm$ 0.5 K offsets to the PSC formation thresholds at each level. Year numbers are for the January of each winter; 2011, 2013, ~~and~~ 2015, and 2016 are highlighted as the blue, orange, green, and red bars, respectively.

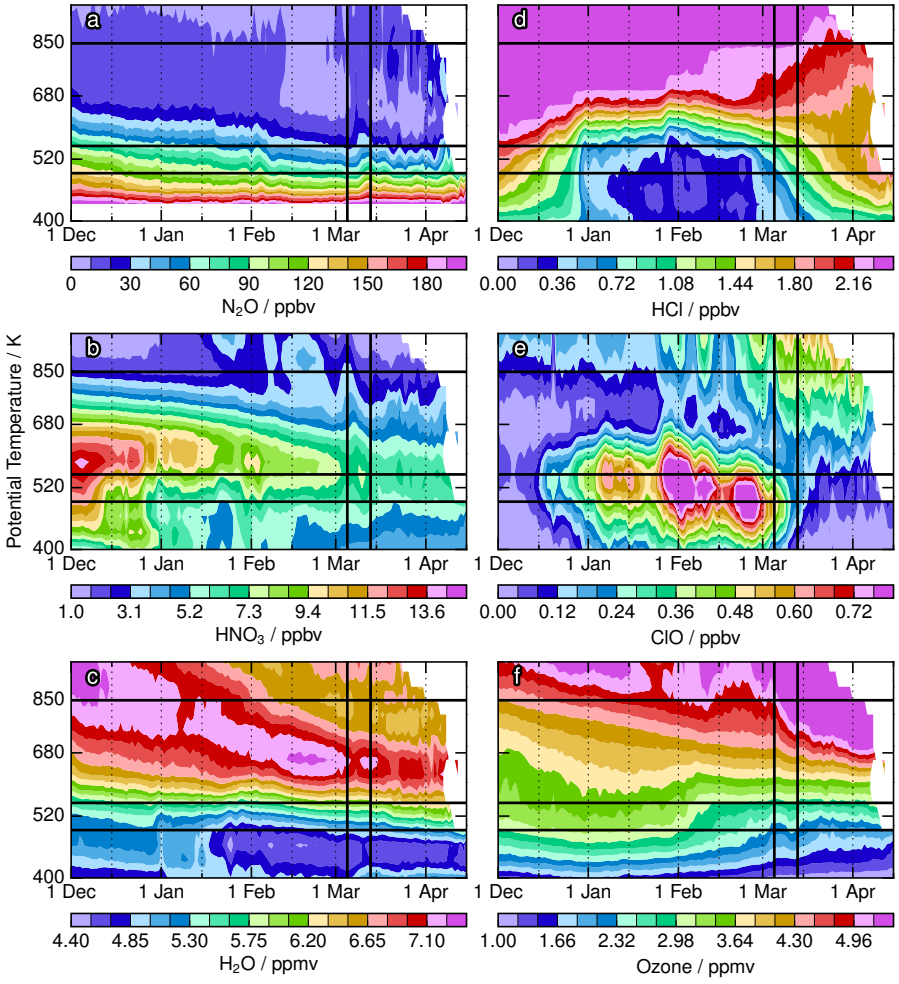

Figure 4. Potential temperature/time series of vortex averaged (the sum of all regions identified by CAVE-ART using the 84°EqL threshold) MLS trace gases during the 2015/16 winter showing N_2O (a), HNO_3 (b), H_2O (c), HCl (d), ClO (e), and ozone (f). Horizontal black lines indicate 490, 550, and 850 K, the primary levels we focus on in this paper. The two black vertical lines indicate the SSW onset, and the ensuing vortex split. Version 4 MLS N_2O at 100 hPa shows unphysical biases (Livesey et al., 2015a); N_2O values below 430 K, where 100 hPa starts to significantly influence the vortex average, are thus not shown.

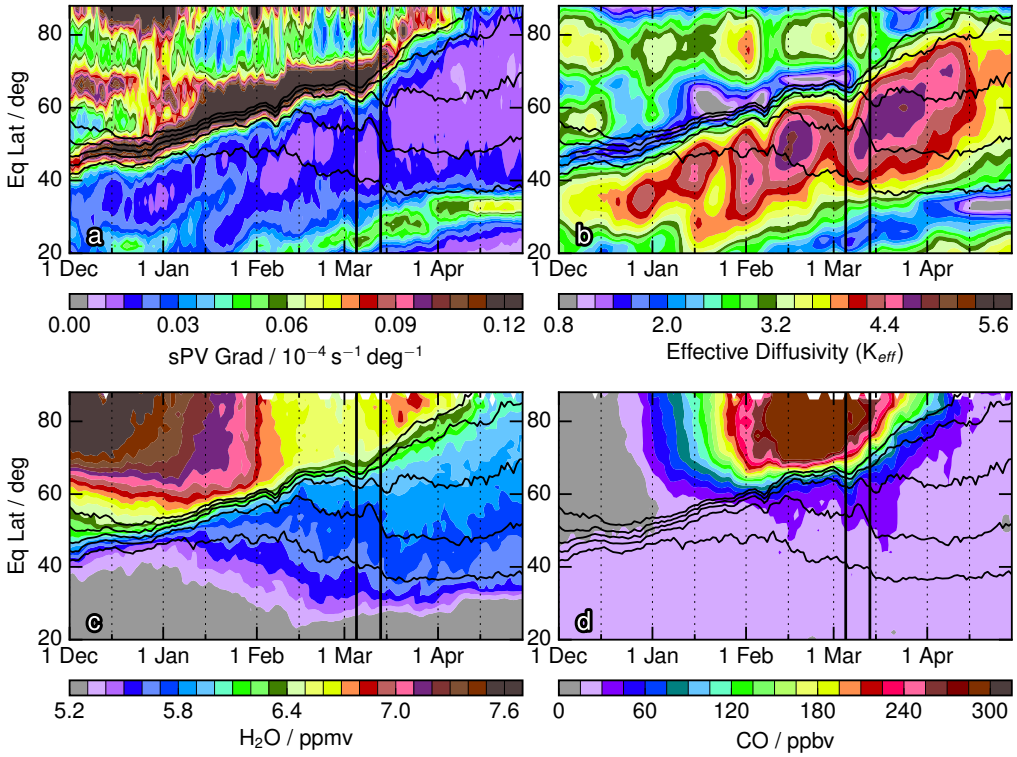

Figure 5. Equivalent latitude/time series at 850 K for 2015/16 showing MERRA-2 (a) sPV gradients and (b) effective diffusivity (K_{eff}), as well as MLS (c) H_2O and (d) CO. Black contours show sPV values of 1.0, 1.2, 1.4, 1.6, and 1.8 $\times 10^{-4}$ s^{-1}in the vortex edge region. The vertical black lines indicate the onset day of the MFW and the following vortex split.

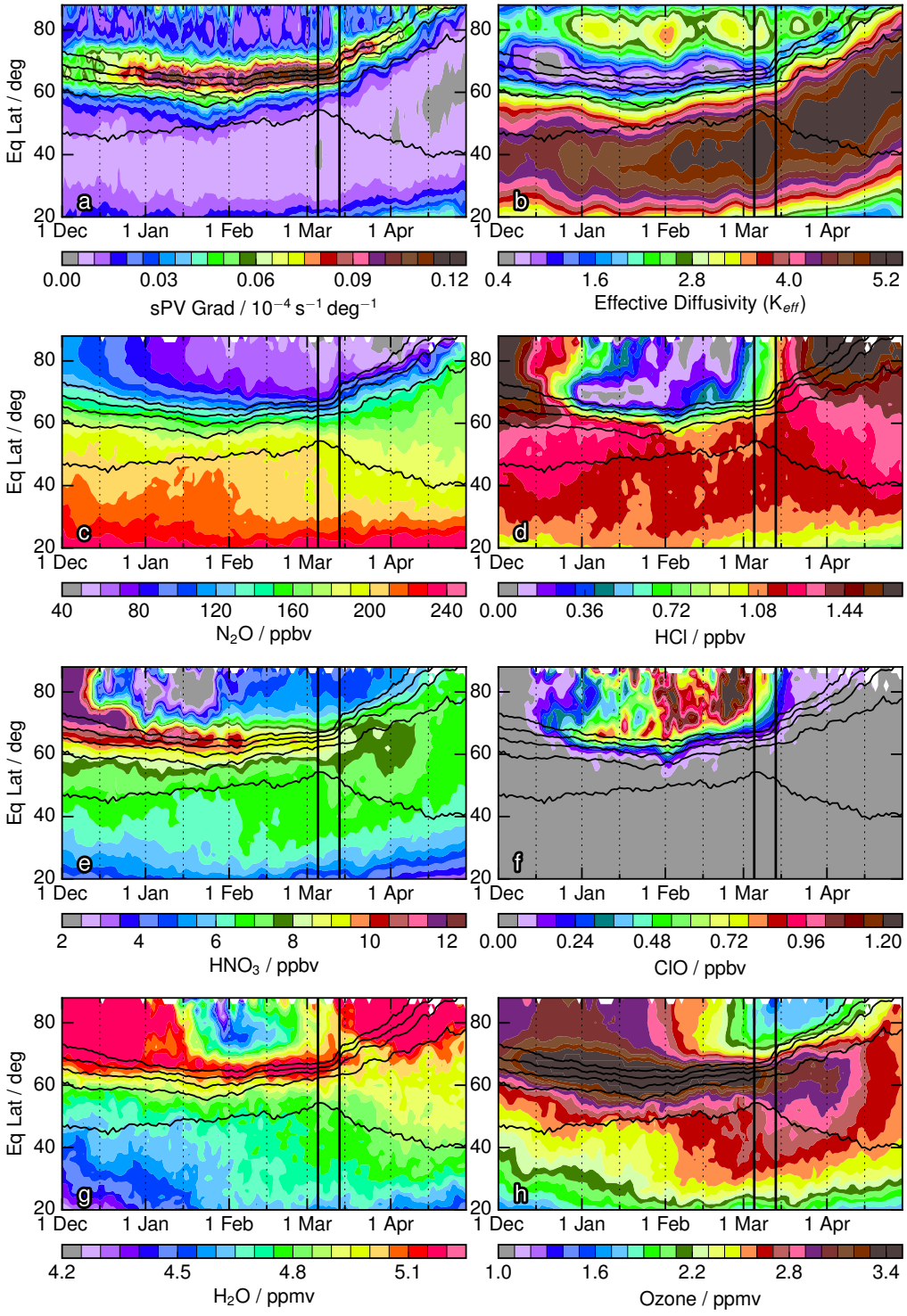

Figure 6. Equivalent latitude/time series at 490 K for 2015/16; as in 5, but showing (a) sPV gradients, (b) K_{eff}, (c) N_2O, (d) HCl, (e) HNO_3, (f) ClO, (g) H_2O, and (h) ozone.

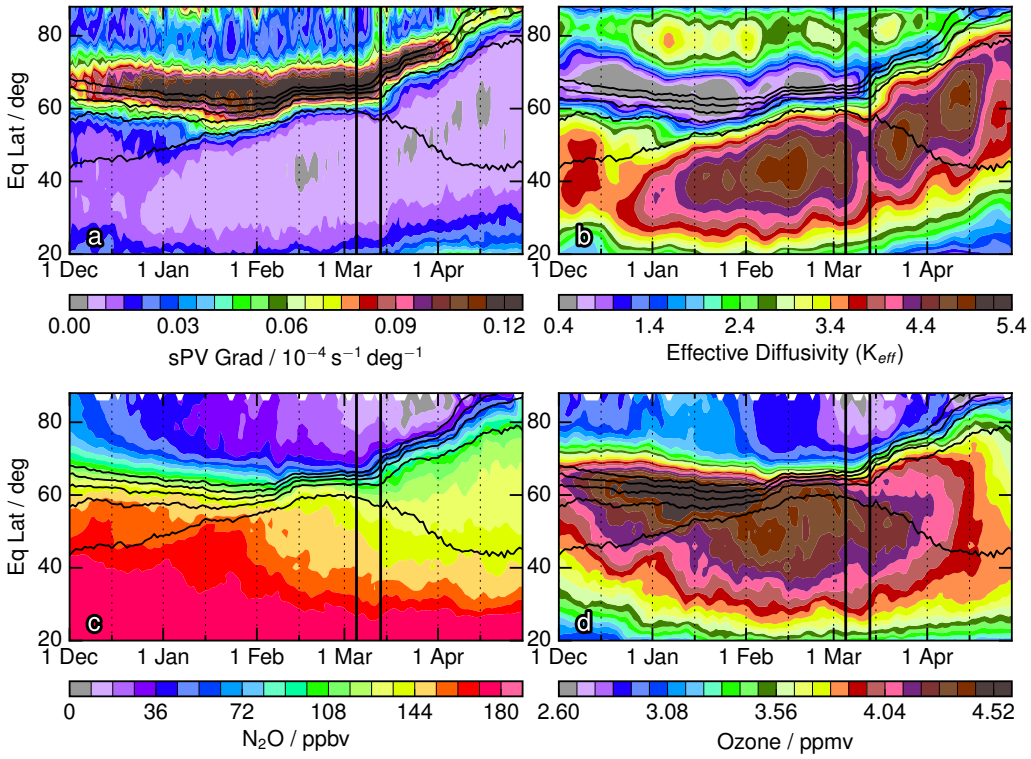

Figure 7. Equivalent latitude/time series at 550 K for 2015/16 as in Figure 6, but showing only sPV gradients (a), K_{eff} (b), N_2O (c), and ozone (d).

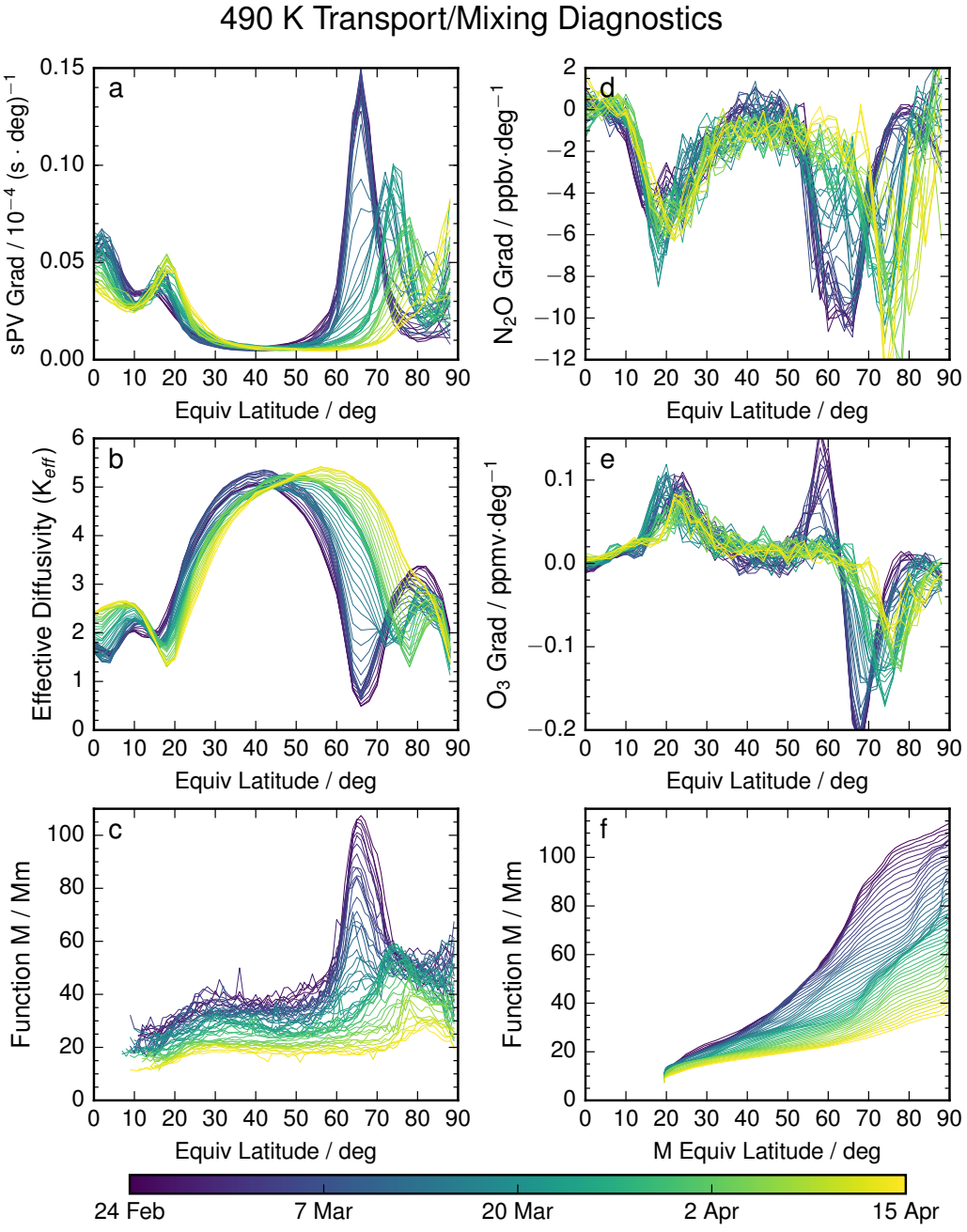

Figure 8. Equivalent latitude line plots of indicators of mixing and transport barriers at 490 K showing individual dates from 24 Feb through 15 Apr (see colorbar). The panels show (a) sPV gradients, (b) K_{eff}, (c) the function M, (d) EqL gradients in N_2O, (e) EqL gradients in ozone, and (f) M as a function of M-based equivalent latitude (M-EqL). Quantities in panels (a) through (e) are all functions of PV-based EqL; panel (f) is the only exception. Note that the units of M are in megameters (Mm, 10^6 m).

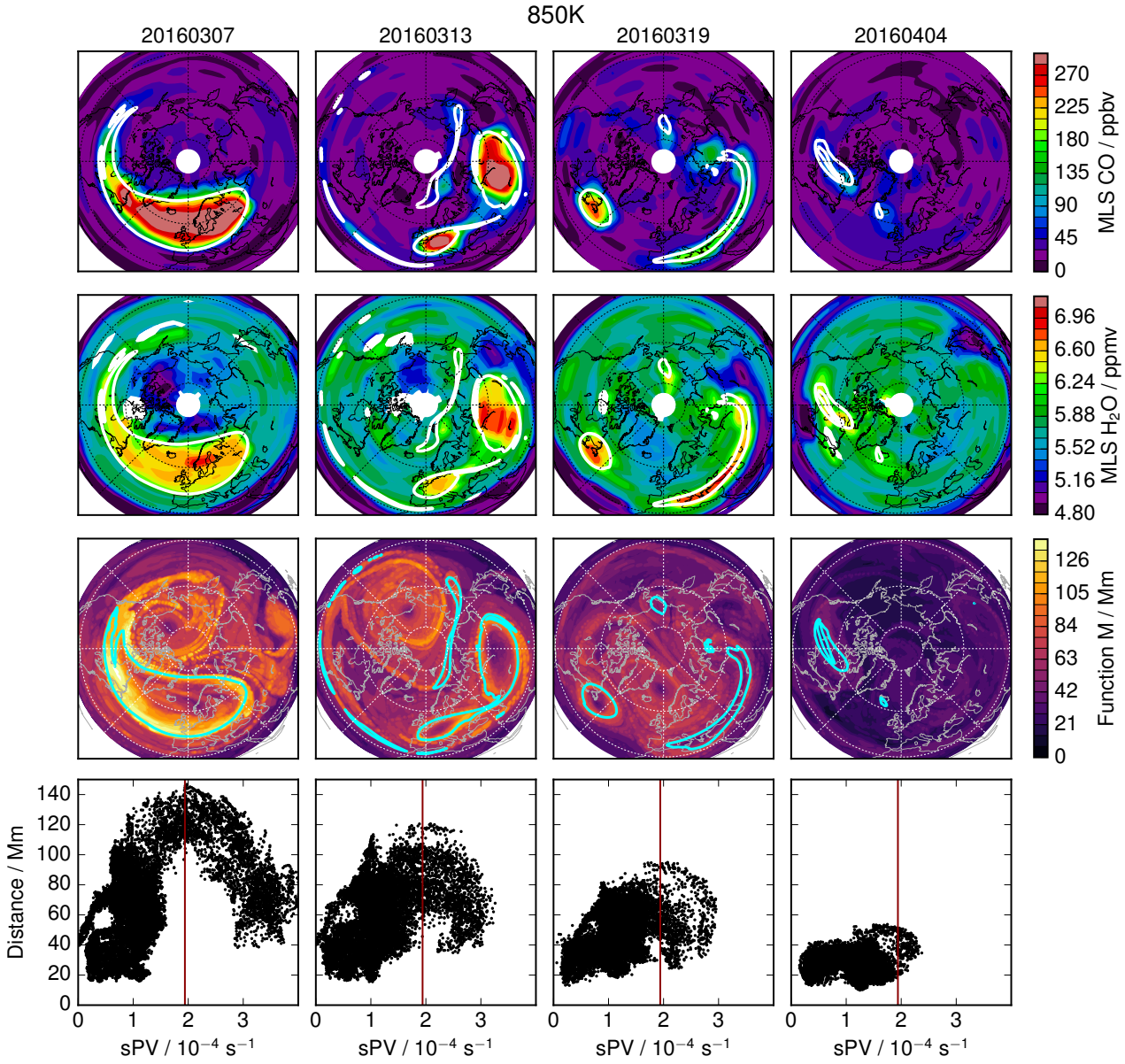

Figure 9. Orthographic maps of 850 K MLS CO (first row) and H_2O (second row), and function M from MERRA-2 (third row), along with scatterplots of M versus scaled potential vorticity (fourth row), for individual dates during the major final warming (columns are 7~~Mar~~ March, 13~~Mar~~ March, 19~~Mar~~ March, and 4~~Apr~~ April, respectively). The white/cyan contours in the ~~first three rows~~maps, and red lines in the bottom row show the sPV value used in CAVE-ART to define the vortex edge at this level. Note that the sPV contours used in the MLS (first two rows) and M (third row) maps are slightly different; the MLS maps show the contour from 12:00UT MERRA-2 PV, whereas the M maps show the value from 00:00 UT (see description of M calculation in section 2.4). Also note that the units of M are in megameters (Mm, 10^6 m). Maps show equator to pole, with 0° longitude at the bottom and 90°E to the right.

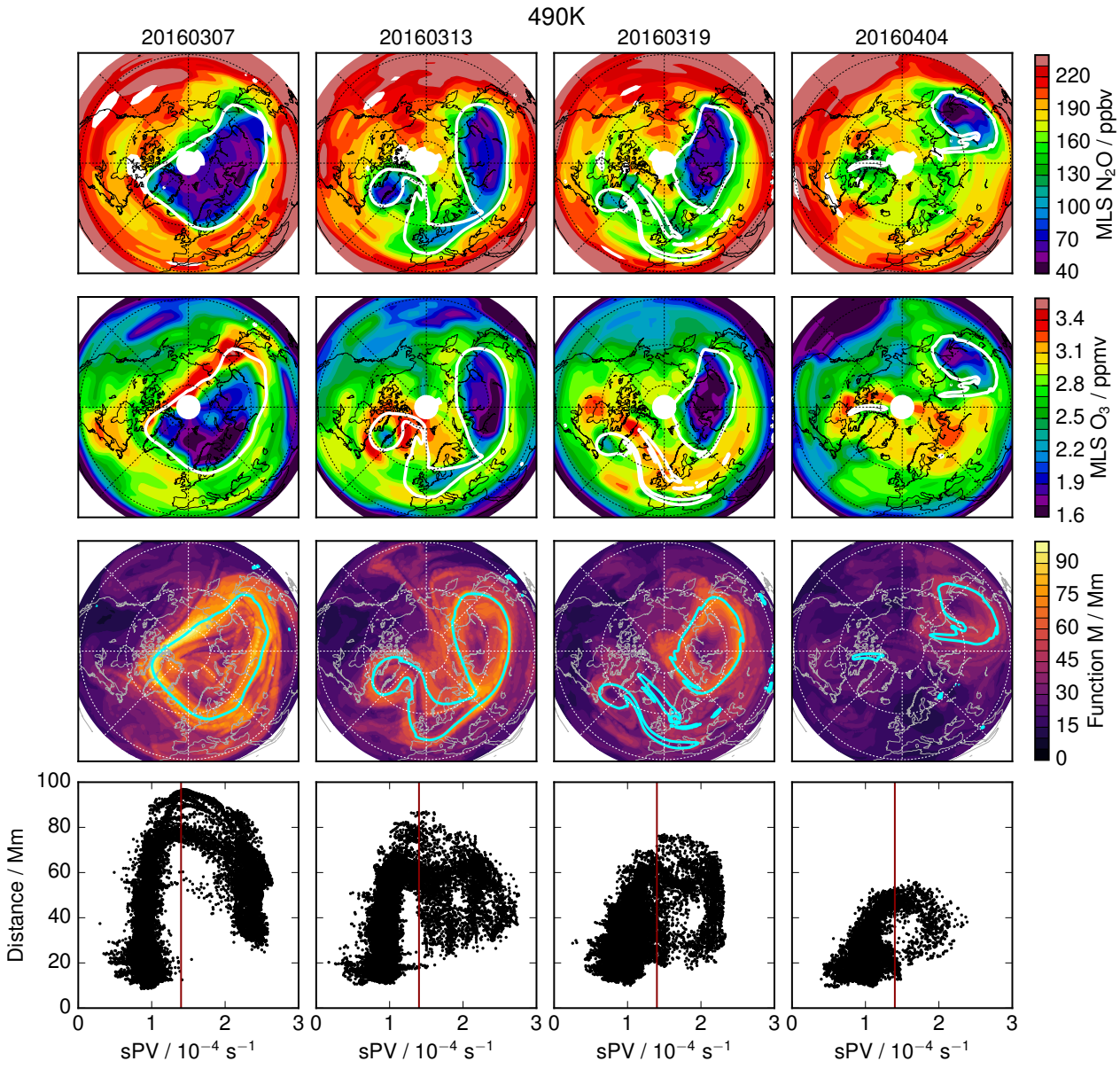

Figure 10. As in ~~Figures~~Figure 9, but at 490 K, and showing MLS N_2O and O_3 (in first and second rows, respectively).

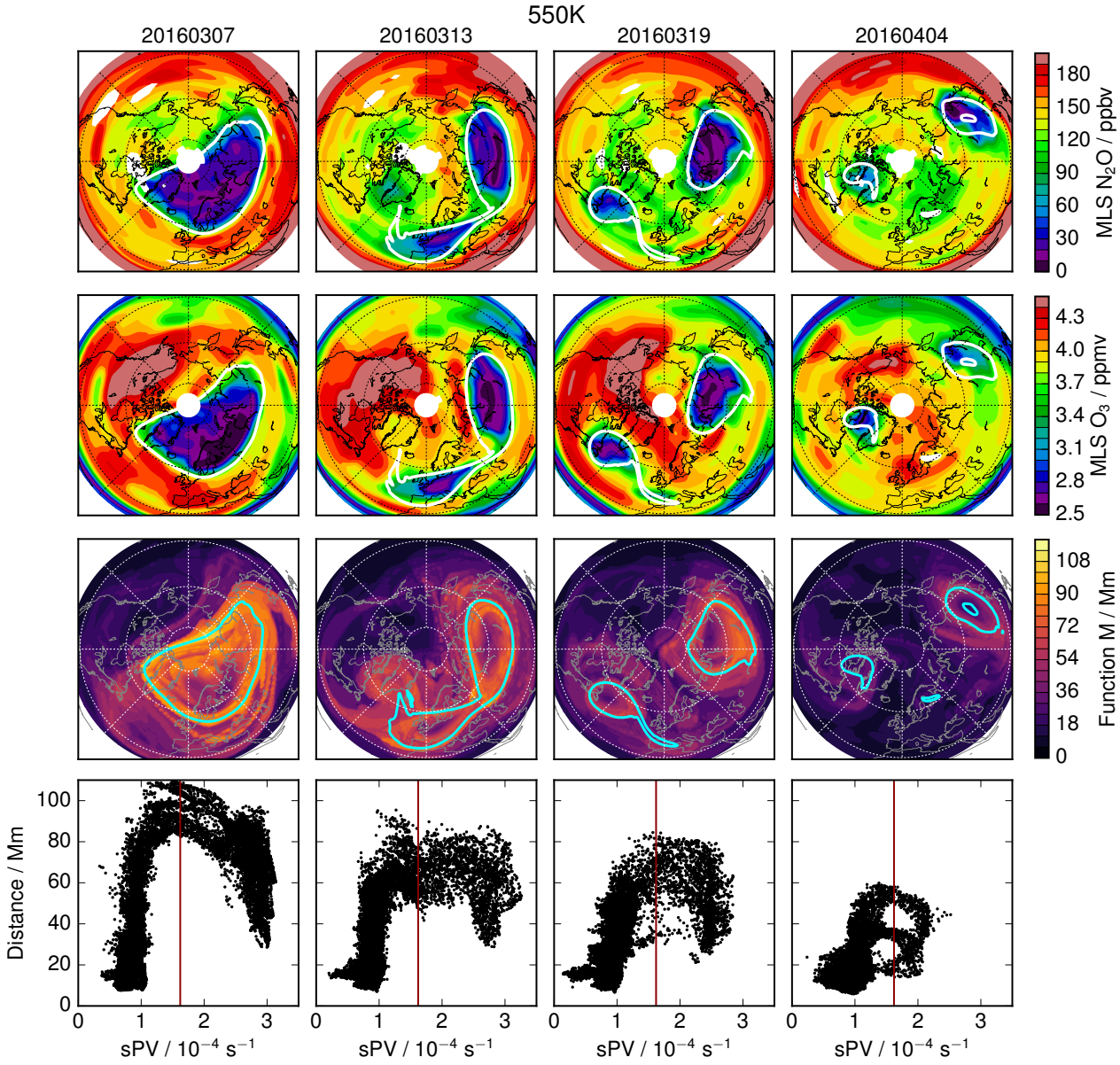

Figure 11. As in Figure 10, but at 550 K. Note that contour ranges are different than at 490 K.

~~Trajectory-based parcel history maps at 850K showing the locations of air parcels initialized inside vortex regions as defined by on 12 March. Parcels are colored green, blue, or black if they were inside a valid vortex region on the initialization date (column 2, red labeling); otherwise the parcels are colored grey. Columns 1, 3, and 4 show the locations of these parcels 14 days before, and 8 and 14 days after initialization, respectively. The red contours show the vortex regions identified by in data (subsampled to match the 1.25° × 1.0° longitude latitude grid used by the trajectory runs) on each date.~~

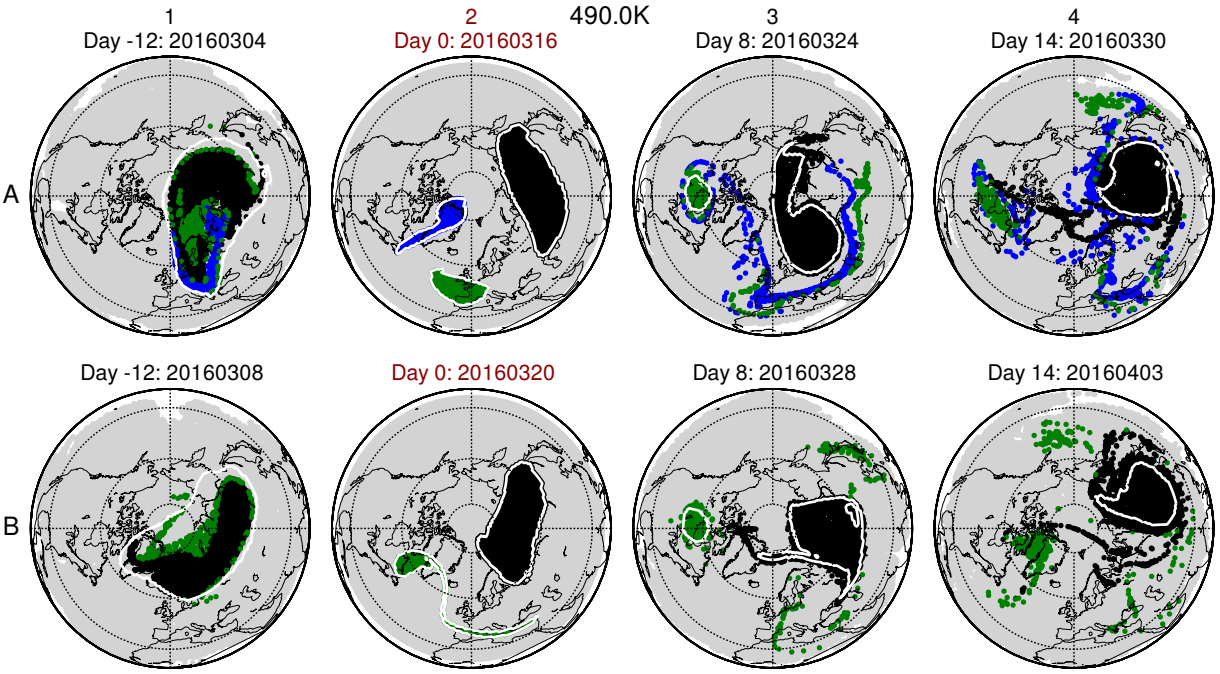

Figure 12. ~~As in Figure ??, but for~~ Trajectory-based parcel history maps at 490 K ~~and~~ showing ~~12 rather than 14 days back~~the locations of air parcels initialized inside vortex regions as defined by CAVE-ART on 16 March (row A) and 20 March (row B). ~~Initialization dates~~ Parcels are colored black (parent), green (offspring-p), or blue (offspring-s) if they were inside a valid vortex region on the initialization date (column ~~2~~, red labeling); otherwise the parcels are ~~16~~ colored grey. Columns 1, 3, and ~~20 March~~ 4 show the locations of these parcels 12 days before, and ~~10 April~~8 and 14 days after initialization, respectively. The white contours show the vortex regions identified by CAVE-ART in MERRA-2 data (subsampled to match the 1.25° × 1.0° longitude/latitude grid used by the trajectory runs) on each date. Maps show equator to pole, with 0° longitude at the bottom and 90°E to the right.

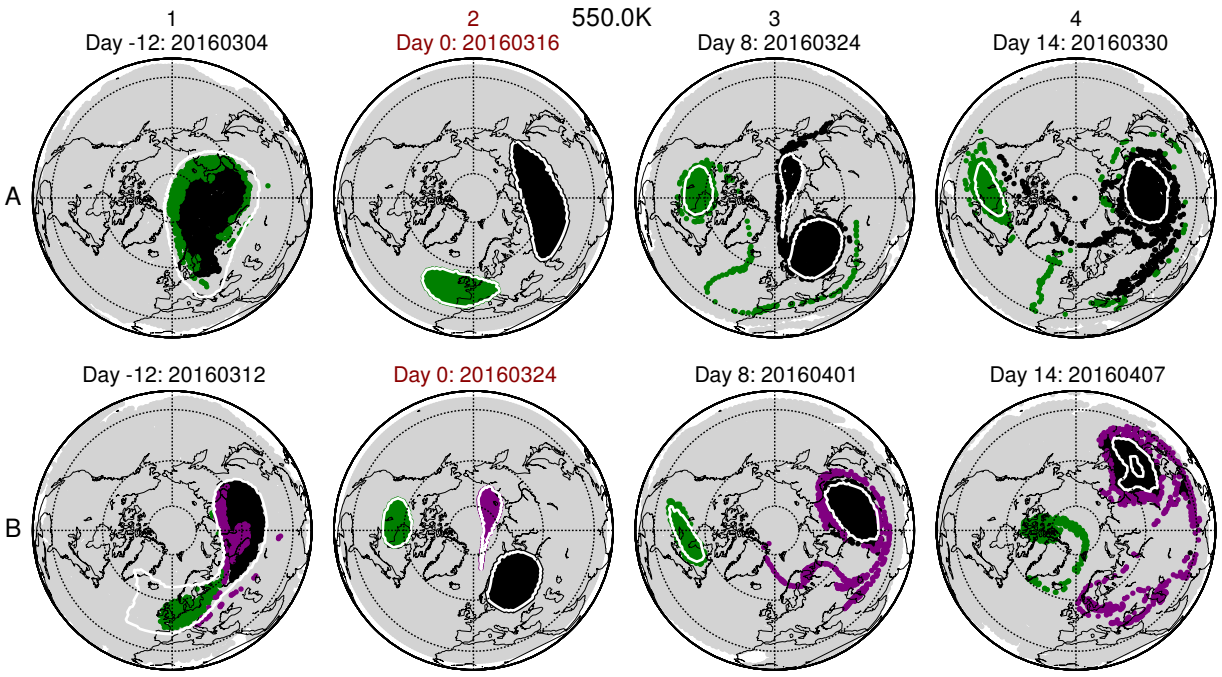

Figure 13. As in Figure 12, but for 550 K ~~. Initialization~~ with 16 and 24 March as the initialization dates (column 2)~~are 16 and 24 March and 6~~. In this case, the purple colored parcels were initialized in a short-lived "transient" vortex, whereas the green region/parcels represents the upward extension of the green (offspring-p) region/parcels shown in Figure ~~April~~12.

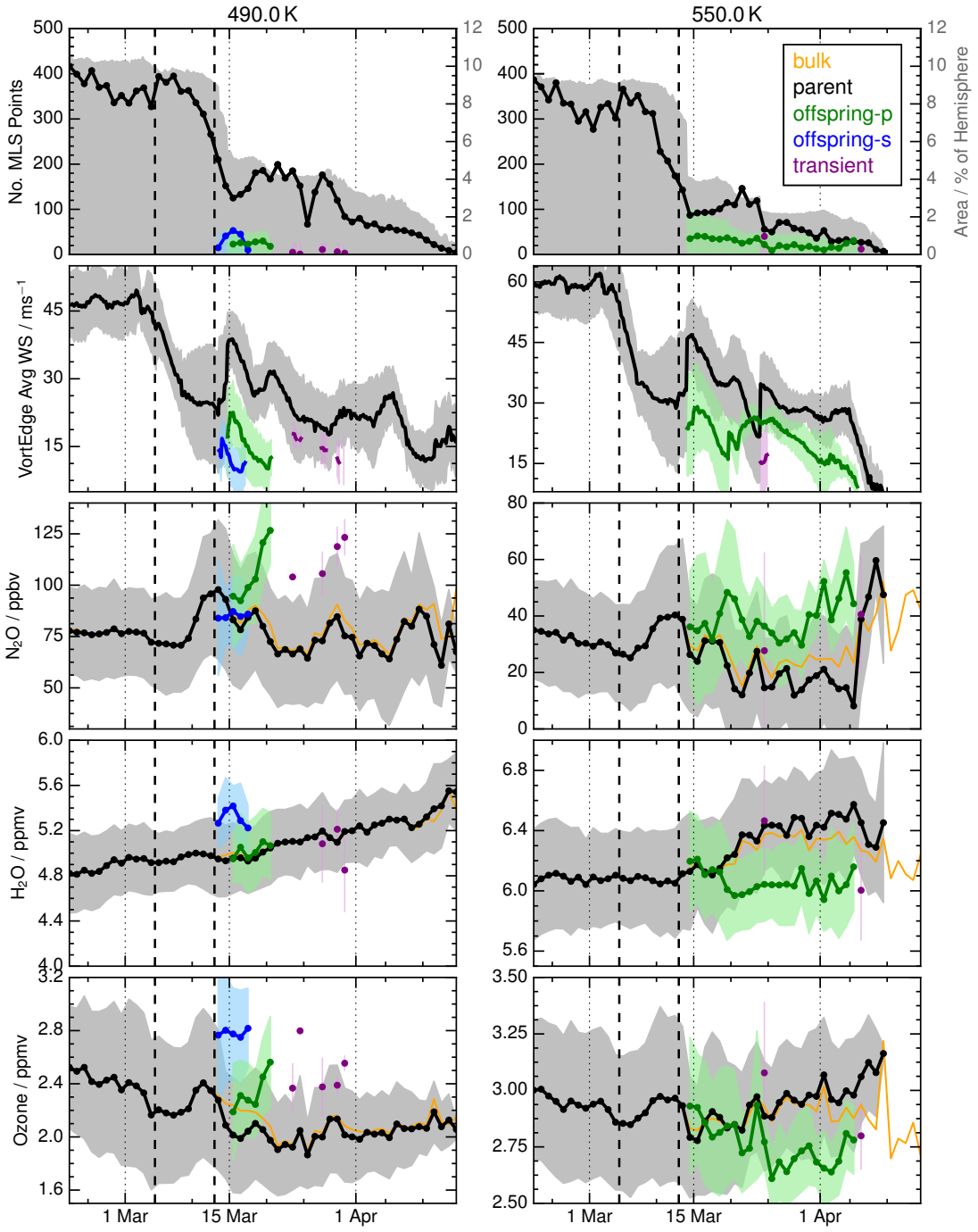

Figure 14. Vortex characteristics and MLS trace gas averages in individual vortex regions in the lower stratosphere. Top panels show the area of each vortex (shading) along with the number of MLS measurement points inside each vortex on each day (lines/symbols). ~~Second~~ The second row shows windspeeds from MERRA-2 averaged around the edge of each individual vortex. Succeeding rows show averages of MLS N_2O (third row), H_2O (fourth row), and ozone (fifth row) in each vortex region. In all rows except the first, ~~with shading indicating~~ the shading indicates ± 1 standard deviation envelopes. In the MLS averages, the ~~dark grey~~ orange lines indicate the "bulk" values (that is, within the vortex edge contour even if the area does not exceed the 84°EqL cutoff, see Section 2.4). In all other cases, the lines are colored/labeled to be consistent with the parcels/regions highlighted in Figures 12 and 13. The offspring vortices are designated "-p" for the more persistent ones and "-s" for the shorter lived ones, as per the discussion of Figures 10 through 13; offspring vortices that persisted for about a day or